



journal homepage: [www.elsevier.com/locate/csbj](http://www.elsevier.com/locate/csbj)



Review

# Delineating the mechanisms and design principles of *Caenorhabditis elegans* embryogenesis using *in toto* high-resolution imaging data and computational modeling



Guoye Guan<sup>a</sup>, Zhongying Zhao<sup>b,c,\*</sup>, Chao Tang<sup>a,d,e,\*</sup>

<sup>a</sup> Center for Quantitative Biology, Peking University, Beijing 100871, China

<sup>b</sup> Department of Biology, Hong Kong Baptist University, Hong Kong 999077, China

<sup>c</sup> State Key Laboratory of Environmental and Biological Analysis, Hong Kong Baptist University, Hong Kong 999077, China

<sup>d</sup> Peking–Tsinghua Center for Life Sciences, Peking University, Beijing 100871, China

<sup>e</sup> School of Physics, Peking University, Beijing 100871, China

ARTICLE INFO

Article history:

Received 26 April 2022

Received in revised form 10 August 2022

Accepted 11 August 2022

Available online 19 August 2022

Keywords:

*Caenorhabditis elegans*

Embryogenesis

*In toto* imaging

Cell lineage tracking

Cell morphology reconstruction

Cell polarization

Mechanical modeling

ABSTRACT

The nematode (roundworm) *Caenorhabditis elegans* is one of the most popular animal models for the study of developmental biology, as its invariant development and transparent body enable *in toto* cellular-resolution fluorescence microscopy imaging of developmental processes at 1-min intervals. This has led to the development of various computational tools for the systematic and automated analysis of imaging data to delineate the molecular and cellular processes throughout the embryogenesis of *C. elegans*, such as those associated with cell lineage, cell migration, cell morphology, and gene activity. In this review, we first introduce *C. elegans* embryogenesis and the development of techniques for tracking cell lineage and reconstructing cell morphology during this process. We then contrast the developmental modes of *C. elegans* and the customized technologies used for studying them with the ones of other animal models, highlighting its advantage for studying embryogenesis with exceptional spatial and temporal resolution. This is followed by an examination of the physical models that have been devised—based on accurate determinations of developmental processes afforded by analyses of imaging data—to interpret the early embryonic development of *C. elegans* from subcellular to intercellular levels of multiple cells, which focus on two key processes: cell polarization and morphogenesis. We subsequently discuss how quantitative data-based theoretical modeling has improved our understanding of the mechanisms of *C. elegans* embryogenesis. We conclude by summarizing the challenges associated with the acquisition of *C. elegans* embryogenesis data, the construction of algorithms to analyze them, and the theoretical interpretation.

© 2022 The Author(s). Published by Elsevier B.V. on behalf of Research Network of Computational and Structural Biotechnology. This is an open access article under the CC BY-NC-ND license (<http://creativecommons.org/licenses/by-nc-nd/4.0/>).

Contents

1. Introduction . . . . .	5501
2. Cellular-resolution studies of embryogenesis. . . . .	5502
2.1. Cell tracing and lineaging. . . . .	5503
2.2. Cell morphology reconstruction . . . . .	5503
2.3. Comparison with other animal models . . . . .	5505
3. Physical models . . . . .	5506
3.1. Reaction-diffusion modeling of cell polarization. . . . .	5506
3.1.1. Known molecular mechanisms . . . . .	5506
3.1.2. Critical role of the mutual inhibition of aPAR and pPAR . . . . .	5508

\* Corresponding authors at: Department of Biology, Hong Kong Baptist University, Hong Kong 999077, China (Z. Zhao). Center for Quantitative Biology, Peking University, Beijing 100871, China (C. Tang).

E-mail addresses: [zyzhao@hkbu.edu.hk](mailto:zyzhao@hkbu.edu.hk) (Z. Zhao), [tangc@pku.edu.cn](mailto:tangc@pku.edu.cn) (C. Tang).

3.1.3. Investigation of additional motifs and regulations. . . . .	5508
3.2. Mechanical modeling of cell positioning and cell morphology . . . . .	5508
3.2.1. Multi-particle model . . . . .	5508
3.2.2. Coarse-grained model. . . . .	5509
3.2.3. Phase field model. . . . .	5510
4. Summary and outlook . . . . .	5511
Funding . . . . .	5511
Declaration of Competing Interest . . . . .	5511
Acknowledgments . . . . .	5511
References . . . . .	5512

## 1. Introduction

*Caenorhabditis elegans* is a transparent free-living nematode that dwells in decaying organic samples in soil and feeds on microorganisms such as bacteria. Its embryogenesis occurs inside an axisymmetric oval egg with a length and width of  $\sim 50 \mu\text{m}$  and  $\sim 30 \mu\text{m}$ , respectively, over a period of 10–12 h at 20 °C [1,2]. After hatching, *C. elegans* grows from  $\sim 250$  to  $\sim 850 \mu\text{m}$  in length via four larval stages and over a period of 44–46 h at 20 °C [1,3]. The tiny size of *C. elegans* means that a microscope is usually needed to observe its anatomy and behavior. Its life cycle from zygote to egg-laying adult is only  $\sim 3$  days at room temperature, and as each individual lays  $\sim 300$  eggs in  $\sim 60$  h, it is an efficient and low-cost organism for biological research, particularly genetics research [1,4]. There are two sexes of *C. elegans*: hermaphrodite and male. Hermaphrodites' progeny generated by self-fertilization are nearly all hermaphrodites with only  $\sim 0.1\%$  males, while those produced by mating are  $\sim 50\%$  males [2]. The hermaphrodite progeny generated by self-fertilization have the same genome as their hermaphrodite parent, which enables molecular biologists to perform experiments with high genotypic and phenotypic stability (Fig. 1A).

Since the early 20<sup>th</sup> century, it has been known that adult *C. elegans* have a constant number of somatic cells; this is an example of the deterministic phenomenon known as eutely [5,6]. Thus, although *C. elegans* has numerous types of organs and tissues, such as the skin, pharynx, neuron, muscle, and gonad, hermaphrodite embryos comprise only 558 living cells and male embryos comprise only 560 living cells, with the corresponding adults comprising 959 and 1,031 cells, respectively [7]. This has enabled every cell's behavior and function during its lifespan to be fully recorded, revealing the highly invariant somatic-cell lineages of the embryonic and postembryonic stages (Fig. 1B) [8–12]. However, *C. elegans* cells do show variations in the timing and orientation of their cell division [13–15]. The variety of cell fates is a consequence of progressive cell-fate specification that occurs after fertilization. First, the zygote (P0) undergoes four successive rounds of asymmetric division to give rise to the soma (i.e., four somatic founder cells: AB, EMS, C, and D) (Fig. 1B). This leaves one remaining germline precursor cell (P4), which undergoes one round of symmetric division to generate two primordial germ cells (Z2 and Z3) [12,16–18]. Second, somatic cells are further differentiated upon induction by cellular signaling, such as by Wnt signaling originating from the embryo posterior, which also induces the asymmetric localization of cellular contents in daughter cells and leads to fate specification [19–21], or by Notch signaling transduced through intercellular physical contact, which drives the differentiation of AB descendants at the 4- and 12-cell stages [22–24]. These stereotypical developmental patterns exhibit the key characteristics of metazoan development, which allows for the study of various biological processes. For instance, in *C. elegans*, there are only two intestinal precursor cells (i.e., Ea and Ep, specified by

Wnt signaling) undergoing gastrulation and there's only one excretory/kidney cell (i.e., ABplpappaap, specified by Notch signaling) [25,26]. In addition, as *C. elegans* has many genes controlling various physiologies and behaviors, it is an excellent animal model for the mechanistic study of many types of processes [27–29]. For example, as a pilot project for the Human Genome Project, the *C. elegans* genome was completely sequenced in 1998. This revealed that its genome consists of  $\sim 19,000$  protein-coding genes, while the number of genes in the human genome was estimated as  $\sim 30,000$ – $40,000$  [30,31]. These studies have required the development of genetic and genomic technologies that, together with sequencing data, have founded a new era of data-driven systems biology studies of worms and other species [32–35]. This has resulted in substantial improvements in our understanding of how genes and proteins function and interact during development and respond to environmental stimuli.

Studies using *C. elegans* have generated several fundamental discoveries that have had significant scientific, social, and economic effects. For example, the 2002 Nobel Prize in Physiology or Medicine was awarded to Sydney Brenner, John E. Sulston, and H. Robert Horvitz, “for their discoveries concerning genetic regulation of organ development and programmed cell death” [36,37]. *C. elegans* was established as a model animal nearly half a century ago by Brenner, who described the induction of *C. elegans* mutants and uncovered its huge pool of genetic units [27,28]. Sulston and co-workers performed laborious naked-eye studies of *C. elegans* to trace its complete cell lineage, from zygote to adult, which serves as a repeatable reference for the migration, division, and differentiation of every *C. elegans* cell [8,9,12]. Horvitz and co-workers exploited the invariant cell apoptosis pattern in *C. elegans* development to identify the “death genes” and “survival genes” that control apoptosis and the genes that regulate the removal of dead cells, which has facilitated much research in developmental and cell biology, especially in cancer biology [38–41]. Subsequently, Andrew Z. Fire and Craig C. Mello were awarded the 2006 Nobel Prize in Physiology or Medicine “for their discovery of RNA interference – gene silencing by double-stranded RNA,” whereby the expression of selected genes is suppressed by double-stranded RNA homologous to these genes' RNA [36,37,42,43]. This gene-knockdown method and cellular-resolution data on the development of *C. elegans* have facilitated high-throughput identification and analysis of cell- and lineage-specific gene functions [15,44–46]. Furthermore, the 2008 Nobel Prize in Chemistry was awarded to Osamu Shimomura, Martin Chalfie, and Roger Y. Tsien “for the discovery and development of the green fluorescent protein, GFP” [36,37]. Chalfie, a neurobiologist, pioneered the use of GFP to visualize gene expression in the mechanosensory neurons of living *C. elegans* larvae, which paved the way for direct monitoring of gene or cellular/tissue activities *in vivo* at both spatial and temporal scales [47]. Thus, the above-mentioned discoveries and technological developments have established a solid foundation for quantitative, systematic, and single-cell-based research on *C. elegans* embryogenesis.

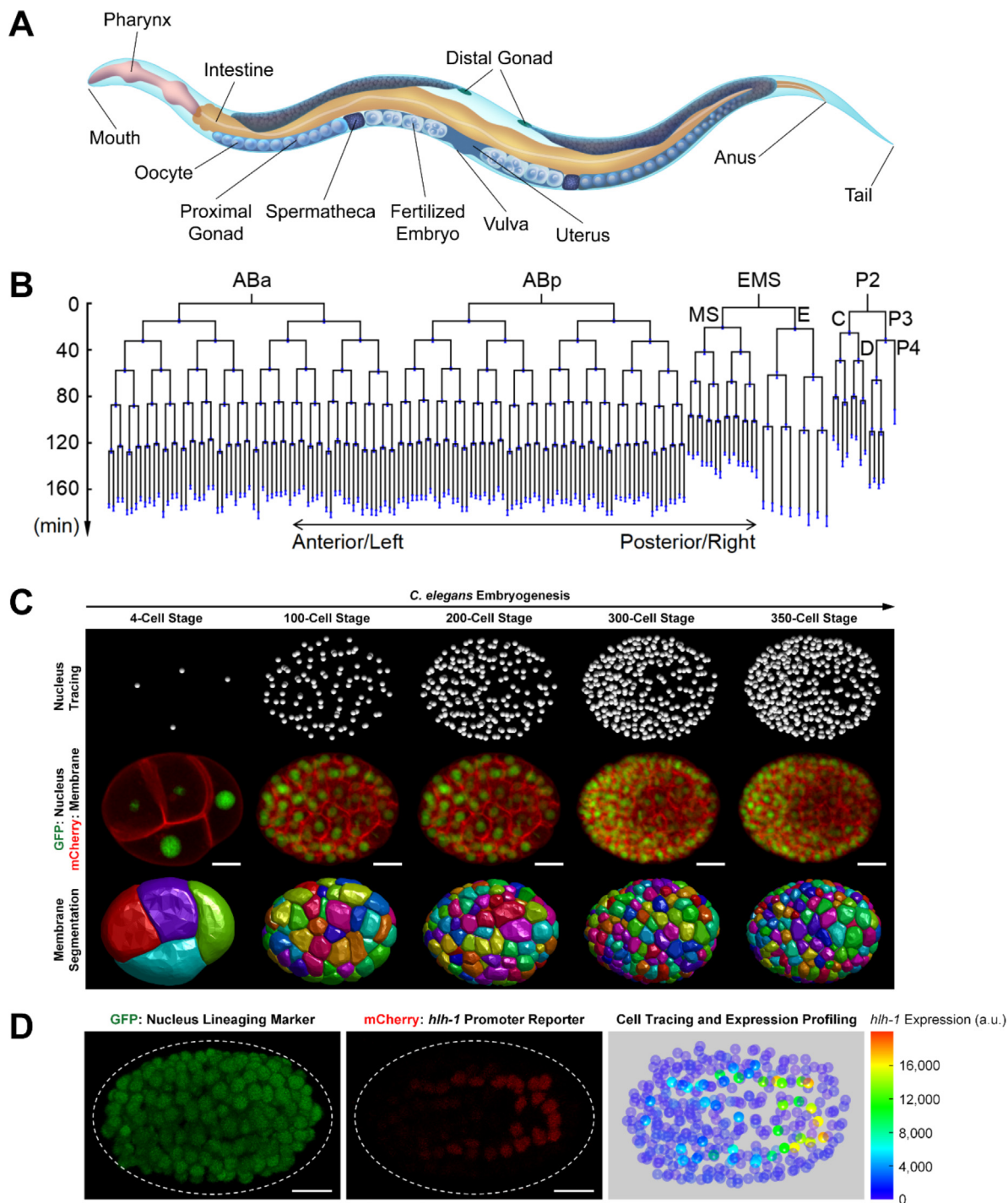


**Fig. 1.** *C. elegans* embryogenesis and cell lineage analysis. (A) Simplified diagram of adult hermaphrodite *C. elegans*. (B) Embryonic cell lineage trees composed of the cells with a complete lifespan recorded from the 4- to 350-cell stages [76]. The branch length (cell cycle length) of the tree is an average of 46 wild-type embryos, and the blue bar at the bottom terminal of each branch denotes the standard deviation of the corresponding cell cycle length. (C) Images of fluorescently labeled cell nuclei and cell membranes (middle row) and the corresponding nucleus tracing (upper row) and membrane segmentation (lower row); a scale bar (white line) denotes 10  $\mu\text{m}$  (the original data are from [76]). (D) Images of cells with fluorescently labeled cell nuclei (left) and *hlh-1* promoter reporters (middle) and the corresponding cell tracing and expression profiling with expression intensity scaling (right); a scale bar as in C (all of these subfigures are reproduced from [67]). (For interpretation of the references to color in this figure legend, the reader is referred to the web version of this article.)

## 2. Cellular-resolution studies of embryogenesis

In this section, we review methods used for cell tracing and lineage tracking (hereinafter referred to as lineaging) and cell morphology reconstruction in *C. elegans*. The developmental

characteristics of and technologies that have been used to study the ascidian, fruit fly, and zebrafish are briefly introduced and compared with the developmental characteristics of and technologies that have been used to study *C. elegans*, to demonstrate its strength as a model system.

## 2.1. Cell tracing and lineaging

Given the nematode species' stereotypical developmental pattern in terms of their cell position, cycle, and fate, it has been recognized that customized methods are needed for tracing nematode cell lineage [5,48–50]. Although it is relatively easy to identify cells in a juvenile or adult nematode, it is extremely difficult to identify cells in a developing embryo, in particular during later embryogenesis when (compared with early embryogenesis) there are more cells and those from the same lineage and with the same fate look similar. This means that researchers must be able to recognize patterns while the blastomere is in rapid cleavage and the cell volume is continuously decreasing. This problem was taken seriously when Sydney Brenner showed his vision in the utility of *C. elegans* in biological research [27–29]. Several of his postdoctoral researchers and others devoted themselves to establishing the cell lineage pattern of *C. elegans* and in around 1980, after years of laborious observation and recording, achieved the historic milestone of a full description of its cell lineage, from zygote to adult. Remarkably, this was achieved using manual techniques, aided by Nomarski microscopy, and it provided a reliable reference for further research using this organism [8–12]. The nomenclature for cell identity was established based on an arbitrary lineal origin and the relative location of offspring cells with respect to the anterior–posterior, left–right, and dorsal–ventral body axes [9,12]. As mentioned, the zygote is named P0, and its successively derived germline precursor cells inherit the prefix “P” and are labeled with a suffix (1–4) to denote their generation. P4 divides symmetrically to produce two primordial germ cells, Z2 and Z3, which then arrest until the larval stage. The somatic founder cells generated by P0, P1, P2, and P3 are named AB, EMS, C, and D, respectively. The daughter cells of a somatic cell take their name from their mother cell's name and its initial location relative to its sister cell (“a” for anterior, “p” for posterior, “l” for left, “r” for right, “d” for dorsal, and “v” for ventral). For example, the daughter cell of AB that is located in the anterior relative to its sister cell is named “ABa,” and the daughters of ABa that are located on either side along the left–right axis are respectively named “ABal” and “ABar.” Hence, all of the cells proliferated throughout *C. elegans* embryogenesis are unambiguously identified and named (Fig. 1B).

Given that manual determination of the entire embryonic cell lineage of *C. elegans* was extremely laborious, it was not feasible to use this approach for determining the entire embryonic cell lineage of a mutant or perturbed embryo [10,12]. In addition, manually collected cell-lineage data are only qualitative or semi-quantitative. However, ~ 15 years after the publication of the pioneering study of Sulston and co-workers, a method for the quantitative tracking of *C. elegans* embryonic cell lineage was developed based on the use of a multifocal-plane time-lapse video recording system and customized tracing/visualizing software, Biocell [13,51]. This method enables systems-level studies, such as cell sorting and developmental variability in each individual cell, with cell nuclei in Nomarski images up to the 400-cell stage used for manual cell identification [52,53]. In 2006, Bao and co-workers developed a platform for automated cell tracing and lineaging called StarryNite, in which cell nuclei are ubiquitously labeled with a histone::GFP fusion protein that increases the contrast between the nuclei and cytoplasm, and thus facilitates segmentation of images acquired by time-lapse three-dimensional (3D) confocal microscopy (Fig. 1C) [54,55]. The labeled nuclei are used for cell identification, which is followed by manual editing to remove errors produced by StarryNite [55,56]. Image acquisition is performed up to the 550-cell stage at 1-min intervals, and these intervals can be reduced to 10 s to observe a transient process [14,15,54,55,57]. The software StarryNite enables the extraction of information on cell position, division timing and axis, and lin-

age/division history from ~ 250 3D time-lapse image stacks consisting of ~ 20,000 two-dimensional (2D) images, while a companion program, AceTree, provides a graphical user interface for manual checking and editing, and visualization and analysis of tracking results (e.g., by plotting a lineage tree) [56]. Manual editing of a 350-cell embryo and a 550-cell embryo can be performed by an expert in 0.5–2 h and 8–16 h, respectively depending on image quality [14,15]. Such cell tracing and lineaging approaches are feasible until the muscle starts twitching [58], as this prevents the acquisition of meaningful images.

The above-described analytical tools have been continually improved to achieve better performance [59–62]. When introducing another fluorescent marker to label the gene of interest by promoter- or protein-fusion, the lineage tracking system is able to generate the lineal of the gene in each cell of a developing embryo [63–66]. As such, the software tool AceBatch was developed to automate this task and adapted to the existing systems constituted by StarryNite and AceTree [64–66]. This is exemplified by the lineal expression profiling of the muscle-specific transcription factor *h1h-1* (Fig. 1D) [67]. Thus far, expression patterns during *C. elegans* development have been collected for thousands of genes, thereby allowing inference of regulatory control in particular pathways [44,45,63–70]. This systems-level approach to the collection of spatial and genomic information is readily adaptable to other nematode species, which has facilitated comparative and evolutionary biology studies [71–73]. Furthermore, cell lineage data obtained by the above-described method have been used to establish statistical references for *C. elegans* embryogenesis to enable cellular-resolution systematic characterization of developmental properties and to build visualization software, such as Dev-scape, WormGUIDES, and STAR [58,74,75]. The above-mentioned analytical tools are summarized in Table 1.

## 2.2. Cell morphology reconstruction

Cell morphology is the 3D space that is surrounded by a cell membrane, and is defined by multiple parameters, including cell shape, volume, surface area and relationship to and area of contact with other cells. Cell morphology is a result of both intracellular and intercellular forces, and experimental and theoretical studies have shown that it reveals the mechanical state of a (multi)cellular system and plays a pivotal role in many critical biological processes during metazoan development [77–84]. During *C. elegans* embryogenesis, cell morphology is involved in many functions. First, cell shape is associated with cell fate and cell lineage. For example, AB and P1 are the first two cells derived from P0, and the descendants of AB are more spherical than those of P1. For

**Table 1**  
Analytical software developed for studies of *C. elegans* embryonic cell lineage.

Software	Functions	References
Biocell	Manual cell tracing and lineaging aided by Nomarski image stacks; visualization of the results of cell tracing and lineaging	[13]
StarryNite	Automated probabilistic cell tracing and lineaging aided by fluorescence-labeled image stacks	[54,55,60,61]
AceTree	Manual editing and visualization of the results of automated cell tracing and lineaging, and gene-expression profiling	[55,56,62]
AceBatch	Automated profiling of cellular expression	[64]
Dev-scape	Systematic visualization of the results of cell tracing and lineaging, and gene-expression profiling	[74]
WormGUIDES	Systematic visualization of the results of cell tracing and lineaging	[58]
STAR	Systematic visualization of the results of cell tracing and lineaging	[75]

instance, the gut cells, a sublineage derived from P1, are roughly cuboid and are packed in a regular array after gastrulation [76,85,86]. Moreover, the severely deformed cell shape that comprises filopodia and lamellipodia structures can mediate the movement of cells, such as ABpl during the left–right asymmetric chiral morphogenesis from the 7- to 8-cell stages [75,76,87,88]. Second, cell volume, which is determined by the symmetric or asymmetric division of a mother cell, influences the nucleus-to-cytoplasm ratio and the molecular contents allocated to the daughter cell, which regulates this cell's fate, cycle length and the robustness of its arrangement [89–92]. Third, cell–cell contact serves as a physical basis for signal transduction between specific cell pairs that regulates the signal-receiving cell's orientation during division (e.g., Wnt signaling from C to ABar at the 8-cell stage) and fate specification (e.g., Notch signaling from MS to ABalp and ABara instead of to ABala and ABarp at the 12-cell stage) [22–24,93]. Moreover, cell–cell contact geometry coordinates the orientation of cells during division by directing cortical myosin flows via intercellular mechanical force [94–96]. These findings highlight the emerging demand for a reliable cell-level-accurate 3D time-lapse morphological atlas of *C. elegans* embryos.

Given that all cell nuclei can be fluorescently labeled and automatically traced in a *C. elegans* embryo, this approach has served as a convenient way to obtain data from which to infer the morphological properties of cells (e.g., their relationships to neighboring cells) in wild-type and mutant *C. elegans* embryos and those of other nematodes. The morphometric inference was first used 25 years ago when the whole-embryo cell lineage, cell division, and cell position during *C. elegans* embryogenesis were documented quantitatively, where the cell–cell contacts could be estimated from nucleus-based cell positions and raw images [13]. Bignone (2001) used these data and distance geometry methods (which had been established for studying protein-folding problems) to systematically predict a cell–cell contact map of *C. elegans* embryo based on the distance between cells defined by nucleus positions [97]. More commonly, 3D cell centers represented by cell nuclei are transformed into cell morphologies via the Delaunay triangulation and Voronoi tessellation approaches. First, each point in a continuous space is assigned to its closest cell (center); second, every cell is allocated a convex polyhedral region, i.e., forming a Voronoi diagram [98–101]. Voronoi diagrams have been widely used in combination with 3D time-lapse cell-nucleus position data of *C. elegans* embryos for characterizing and visualizing embryonic morphology, which has greatly facilitated studies in many areas of biology [75,102–113]. Moreover, this implementation has been used to delineate several key mechanisms in *C. elegans* embryogenesis that are supported by experimental evidence, such as Notch signaling and the positional variability mediated by physical contact, cell adhesion, and gap junctions [109,110].

However, although the generation of a Voronoi diagram is an efficient way to process and depict temporal series of 3D images that contain hundreds of cell nuclei, it is an indirect inference of cell surface and thus has inherent disadvantages [114]. First, it identifies two cell nuclei dividing during cytokinesis as separate cells, even though they remain within the membrane of their mother cell. Second, the nucleus inside a cell can exhibit drastic movement without the body or shape of the cell being obviously affected, especially during the mitotic process [115,116]. Third, a Voronoi diagram partitions space into convex polyhedra with planar surfaces, whereas a deformed cell may have severely curved and irregular surfaces [76,87,88]. Fourth, the partitioned polyhedra are packed tightly against those representing neighboring cells, which means that an authentic anuclear cavity, such as a blastocoel, cannot be established [117]. Thus, a Voronoi analysis usually requires a large sample size of cells or embryos to reach sufficiently high statistical reliability and, when applied to a cell-specific prob-

lem, must be checked by comparison with direct observations of membrane morphology to avoid the generation of false-positive or false-negative results [109].

A few studies have extracted cell morphology based on empirical data on cell membranes acquired by general image segmentation software or manual annotation [89–91,107,118]. However, although *C. elegans* cell membranes can be tagged with a fluorescent marker to enable cellular boundaries to be determined, existing image-segmentation methods are difficult to apply to the labeled *C. elegans* embryos due to their relatively small size. Therefore, there is an urgent need for an automatic, reliable, and efficient segmentation tool for studies of *C. elegans* cellular morphology. Accordingly, in the past 5 years, many researchers have developed experimental methods to label cell membranes with fluorescent proteins and designed new segmentation algorithms customized for processing 3D time-lapse series of images of *C. elegans* embryogenesis (Table 2) [76,109,119–122]. In 2017, Azuma *et al.* reported the cell segmentation software named Biologically Constrained Optimization-based cell Membrane Segmentation (BCOMS), in which biological knowledge is included as a constraint in the segmentation process, i.e., it is assumed that the embryo size is nearly invariant and the nucleus is surrounded by a cell membrane [119]. In the evaluation of 25 shape features, this method exhibited an average deviation of 5.6 % from the results generated by manually annotating a 24-cell-stage embryo. In 2019, Cao *et al.* integrated several existing algorithms to preprocess raw images before watershed segmentation and devised a computational pipeline named 3D Membrane Morphological Segmentation (3DMMS) [120]. For *C. elegans* embryogenesis up to the ~86-cell stage, the dice ratio (i.e., the overlap between segmentation output and ground truth) of 3DMMS ( $\geq 0.97$ ) is greater than that of BCOMS. In another vein, Thiels *et al.* designed the pipeline spheresDT/Mpacts-PiCS and showed that a mechanical model considering intracellular and

**Table 2**  
Comparison of algorithms used for reconstructing cell morphology during *C. elegans* embryogenesis.

Algorithm	Information source for segmentation	Features	References
Voronoi diagram	Nucleus	Computationally efficient; capable of processing the entire embryogenesis up to muscle twitching	[75,102–113]
BCOMS	Membrane	Aided by prescribed biological constraints (i.e., the nucleus is surrounded by the membrane and the embryo size is almost unchanged over time)	[119]
3DMMS	Membrane	Integration of existing approaches to preprocess the raw images before segmentation (i.e., statistical intensity normalization, Hessian matrix enhancement, region filter, and surface regression)	[120]
spheresDT/Mpacts-PiCS	Membrane	Morphology refinement with a mechanical model that considers aspects such as cell surface tension, intracellular pressure, and intercellular force	[122]
CShaper	Membrane	Based on deep learning; when combined with the nucleus position, this algorithm is capable of identifying the cavity inside an embryo	[76]

intercellular forces can substantially refine the segmented cell morphologies [122–124]. It's a remarkable finding that cell mechanics—which are difficult to directly observe or measure *in vivo*—can be inferred from a combination of an appropriate mechanical model and 3D cell-membrane images [122,125,126].

CShaper is a novel segmentation algorithm based on deep learning that takes advantage of a new transgenic strain of *C. elegans* that ubiquitously expresses GFP in nuclei and the red fluorophore mCherry in cell membranes during embryogenesis (Fig. 1C) [76]. CShaper performs automated segmentation of cell membranes to reconstruct cell morphology during *C. elegans* embryogenesis. Thus, in combination with an automated lineaging algorithm, CShaper enables the automated generation of cellular morphologies and the resolution of cell identities from the 4- to 350-cell stages at an interval of  $\sim 1.5$  min [76]. Evaluations of dice ratios, Hausdorff distances (i.e., the largest distance from a voxel in the segmented region to its closest voxel in the ground truth region), and  $F_1$  values (i.e., the proportion of correctly segmented cells) have demonstrated that CShaper outperforms five existing segmentation algorithms (3DUNet, CellProfiler, FusionNet, RACE, and SingleCellDetector) when applied to the *C. elegans* embryo [127–131]. This increased performance of CShaper is due to its deep learning architecture, the large sample size it uses for training, and its customization to *C. elegans* embryogenesis. For example, for a specific time point, over 95 % of cells are segmented before the 200-cell stage, although the loss ratio increases to 18 % during the 200- to 350-cell stages. In addition, CShaper can reconstruct the cavities inside an embryo, i.e., the non-nucleated empty space, from tracked cell-nucleus positions. Thus, 17 wild-type embryos have been imaged, segmented, and linearly normalized to form a statistical reference consisting of quantitative morphological information, such as cell volumes, cell surface areas, cell–cell contact relationships, and areas, which has been publicly documented as a resource. Each embryo was imaged and segmented until the complete divisions of AB128 (which reach the ninth generation of the AB lineage and yield 256 progeny), MS16 (which reach the sixth generation of the MS lineage and yield 32 progeny), E8 (which reach the fifth generation of the E lineage and yield 16 progeny), C8 (which reach the fifth generation of the C lineage and yield 16 progeny), D4 (which reach the fourth generation of the D lineage and yield 8 progeny), and germline precursor cell P4 (which yields 2 progeny) (Fig. 1B). As a result, a list of cells that each have 17 morphological trajectories were generated, with the smallest cell having an average volume of  $\sim 8.5 \mu\text{m}^3$ . The reference validates 10 cell–cell contacts that have been proposed to be involved in signaling, quantifies the variability of cell size (volume and surface area) and cell–cell contacts (relationship, area, and duration), and shows that cell irregularity is lineage-dependent and likely coupled with cell motility.

Currently, membrane-based cell morphology remains unclear beyond the 350-cell stage in the *C. elegans* embryo, where many morphogenetic events (e.g., ventral cleft closure, dorsal intercalation, epidermal enclosure, elongation, and most apoptosis) occur [132]. The methodology of cell tracing and lineaging for late developmental stages has been established in nematode species because the fluorescently labeled nucleus signal is localized and thus there is a high signal–noise ratio [65,133–135]. However, beyond the 350-cell stage, the performance of membrane-based image segmentation decreases drastically over time, irrespective of the algorithm used. Consequently, there are four major challenges in the reconstruction of cell morphology: (1) the cell volume becomes exponentially smaller but the image resolution of microscopy remains constant over embryo development; (2) scattering and loss of laser intensity through the embryo body decrease image













quality, especially in images of the last focal plane to be collected; (3) resolution of the z-axis (in the axial direction) is much lower than that of the x- and y-axes (in the lateral directions), resulting in blurred images for the cell boundary that is parallel to a focal plane; and (4) the embryo boundary is formed by only a single layer of the fluorescently labeled cell membrane, whereas the cell–cell interfaces inside an embryo consist of two layers of membrane, so the membranes of cells located on an embryo surface are more difficult to be correctly segmented (due to reduced fluorescence intensity) than those of cells inside an embryo. In principle, higher-quality images could be obtained by increasing laser intensity; however, this increases phototoxicity, which may perturb normal development, and increases the photobleaching of fluorescent proteins. Finally, compared with other organisms' embryonic cells, the relatively smaller size of *C. elegans* embryonic cells presents a significant challenge to both fluorescence imaging and image segmentation. Technology improvements in all of the above-mentioned aspects are necessary for enabling the reliable reconstruction of 3D time-lapse cell morphology in the late embryonic development of *C. elegans*.

In terms of algorithmic improvements, one possible strategy could be to consolidate the advantages of various segmentation algorithms, such as those involving deep learning, biological constraints, and mechanical modeling (Table 2). In terms of imaging improvements, the performance of cell segmentation would be enhanced in a *C. elegans* strain that expressed a more uniform and brighter membrane tag across developmental stages and cell types than current strains. In addition, compared with confocal microscopy, Light Sheet Fluorescence Microscopy (LSFM) has a faster imaging speed and causes less phototoxicity and photobleaching, while Structured Illumination Microscopy (SIM) has a resolution approaching the diffraction limit [136–139]. Thus, to further improve the performance of segmentation, image acquisition should be explored using LSFM-based and SIM-based imaging systems that have been developed and adapted for *C. elegans* embryogenesis, such as inverted selective plane illumination microscopy, dual-view inverted selective plane illumination microscopy, and instant structured illumination microscopy [111,140–147].

### 2.3. Comparison with other animal models

Cell tracing and lineaging and cell morphology reconstruction have also been performed in organisms other than *C. elegans*, such as two other invertebrates—the ascidian *Phallusia mammillata* and the fruit fly *Drosophila melanogaster*—and a vertebrate, the zebrafish (*Danio rerio*) (Table 3). Like that of *C. elegans*, the embryonic development of *P. mammillata* involves an invariant cell lineage and cell-level stereotypic spatial patterns, i.e., each cell can be uniquely identified in different embryos based on its reproducible developmental behaviors, such as fate and position [77,148,149]. The *P. mammillata* cell lineage was traced up to its tailbud stage (the  $\sim 850$ -cell stage) based on nucleus recognition using the software Mov-IT [150]. In addition, *P. mammillata* cell-membrane segmentation was achieved up to the neurula stage (the  $\sim 750$ -cell stage) using images obtained with multiview light-sheet microscopy [77], which is around twice the number of cells for which this has been achieved in *C. elegans*. However, (1) the volume of the *P. mammillata* embryo is  $\sim 60$ – $70$  times that of *C. elegans*, meaning that the smallest *P. mammillata* cell that can be segmented is much larger than that of *C. elegans*; and (2) rigorous manual curation must be incorporated into the *P. mammillata* cell membrane-segmentation procedure. Cell morphology reconstruction was also attempted in *D. melanogaster*. Compared with *C. ele-*

**Table 3**  
Developmental characteristics and technical limits of cell tracing and lineaging and cell morphology reconstruction in four widely used animal models.

Organism	Morphological change during development			Developmental characteristics	Terminal cell number for cell tracing and lineaging	Terminal cell number and smallest cell volume for cell morphology reconstruction
	Zygote	Onset of Morphogenesis	Adult			
Nematode ( <i>Caenorhabditis elegans</i> )				Invertebrate; with invariant cell lineage and cell-level stereotypical spatial patterns	~ 550 cells (prior to muscular twitching) [54–56]	~ 350 cells (completion of gastrulation); ~ 8.5 $\mu\text{m}^3$ [76]
Ascidian ( <i>Phallusia mammillata</i> )				Invertebrate; with invariant cell lineage and cell-level stereotypical spatial patterns	~ 850 cells (tailbud stage) [150]	~ 750 cells (neurula stage); ~ 350 $\mu\text{m}^3$ [77]
Fruit fly ( <i>Drosophila melanogaster</i> )				Invertebrate; without invariant cell lineage and cell-level stereotypical spatial patterns	>6,000 cells (Stage 11) [153]	~ 6,000 cells (Stage 6); ~ 450 $\mu\text{m}^3$ [130,154]
Zebrafish ( <i>Danio rerio</i> )				Vertebrate; without invariant cell lineage and cell-level stereotypical spatial patterns	~ 9,500 cells (segmentation period) [150]	~ 5,500 cells (gastrula period); ~ 450 $\mu\text{m}^3$ [130]

Note: The first and second columns of this table are adapted from [157,158], except those for *P. mammillata* [156], and the second column depicts the embryonic stages when zygotic transcription is essential. The smallest cell volume for cell morphology reconstruction represents the smallest cell reported to have been segmented. The value listed for *D. melanogaster* is obtained from the segmentation outputs of RACE [130], and this value is assumed to apply to *D. rerio* as well, considering that the same microscopy method and segmentation algorithm was used for both species.

*gans* and *P. mammillata*, *D. melanogaster* has a much larger embryo and its cell lineage and spatial patterns are not invariant at the cellular level. After fertilization, *D. melanogaster* undergoes 13 rounds of pseudo-synchronous divisions to form a syncytium, followed by blastoderm cellularization involving ~ 6,000 cells (Stage 5), and subsequently gastrulation onset (Stage 6) [151,152]. Whole-embryo cell segmentation has been achieved up to *D. melanogaster* gastrulation (Stage 6), and nucleus-based cell tracing has been attempted up to Stage 11, when the germ band is subdivided into metameric units by parasegmental furrows [130,151,153,154]. However, cell identity is only partially determinable in a *D. melanogaster* embryo as cell tracing and lineaging are not achievable in the first several rounds of cell cycles post-fertilization, as during this period the cells are sparsely located inside the embryo instead of on the periphery of the embryo and are thus difficult to distinguish. Automated reconstruction of cell morphology has also been attempted in *D. rerio*. The software RACE has been developed to extract cell morphology from *D. rerio* embryos in the gastrula period (the ~ 5,500-cell stage, 6 h after fertilization), and Mov-IT has been developed to perform nucleus tracing up to the segmentation period (the 9,500-cell stage, 11 h after fertilization) [130,150,155].

Although automated cell tracing and lineaging and cell morphology reconstruction are feasible in all four animal models, *C. elegans* embryogenesis has the most condensed developmental trajectories out of all organisms. For instance, *C. elegans* gastrulation begins at the 26-cell stage, while *P. mammillata* gastrulation begins at the 112-cell stage, and both *D. melanogaster* and *D. rerio* gastrulations begin after thousands of cells are formed [117,150,152,156]. Moreover, *C. elegans* embryogenesis ends with ~ 550 living cells, the identity of each of these can be resolved by nucleus-based cell tracing and lineaging, and the fate of each of these has been documented [12,54–56]; this can be advantageous for systematically studying developmental events at the cellular level. Thus, researchers studying *C. elegans* to answer various ques-

tions in metazoan embryogenesis may benefit by focusing on only a single cell or all cells in an embryo.

### 3. Physical models

In this section, we review the application of physical models for elucidating two biological phenomena, i.e., cell polarization and morphogenesis, and understanding the underlying genetic programs selected by evolution.

#### 3.1. Reaction-diffusion modeling of cell polarization

Cell polarization is responsible for many significant biological processes in the zygote, in germline precursor cells, and in their derived somatic cells during *C. elegans* embryogenesis [159,160]. Cell polarization in P0–P3 occurs sequentially, and many of its associated regulatory pathways have been revealed by experiments. Thus, the cell polarization in those cells has served as the basis for theoretical studies in recent years.

##### 3.1.1. Known molecular mechanisms

Cell polarization plays a decisive role in the segregation of cell contents, the orientation of cell division, and the specification of cell fate and has therefore been a focus in developmental biology for many years (reviewed in [161]). Four consecutive rounds of asymmetric divisions governed by cell polarization occur in P0, P1, P2, and P3 during *C. elegans* embryogenesis, thereby providing a framework for research on cell polarization (Fig. 2A) [162]. In each asymmetric division, a new somatic founder cell is generated, while the other daughter cell—the next P cell—remains multipotent. After that, the last P cell, P4, undergoes symmetric division and yields two primordial germ cells, Z2 and Z3, due to its too small size and loss of cell polarity [163]. Cell polarity is first estab-

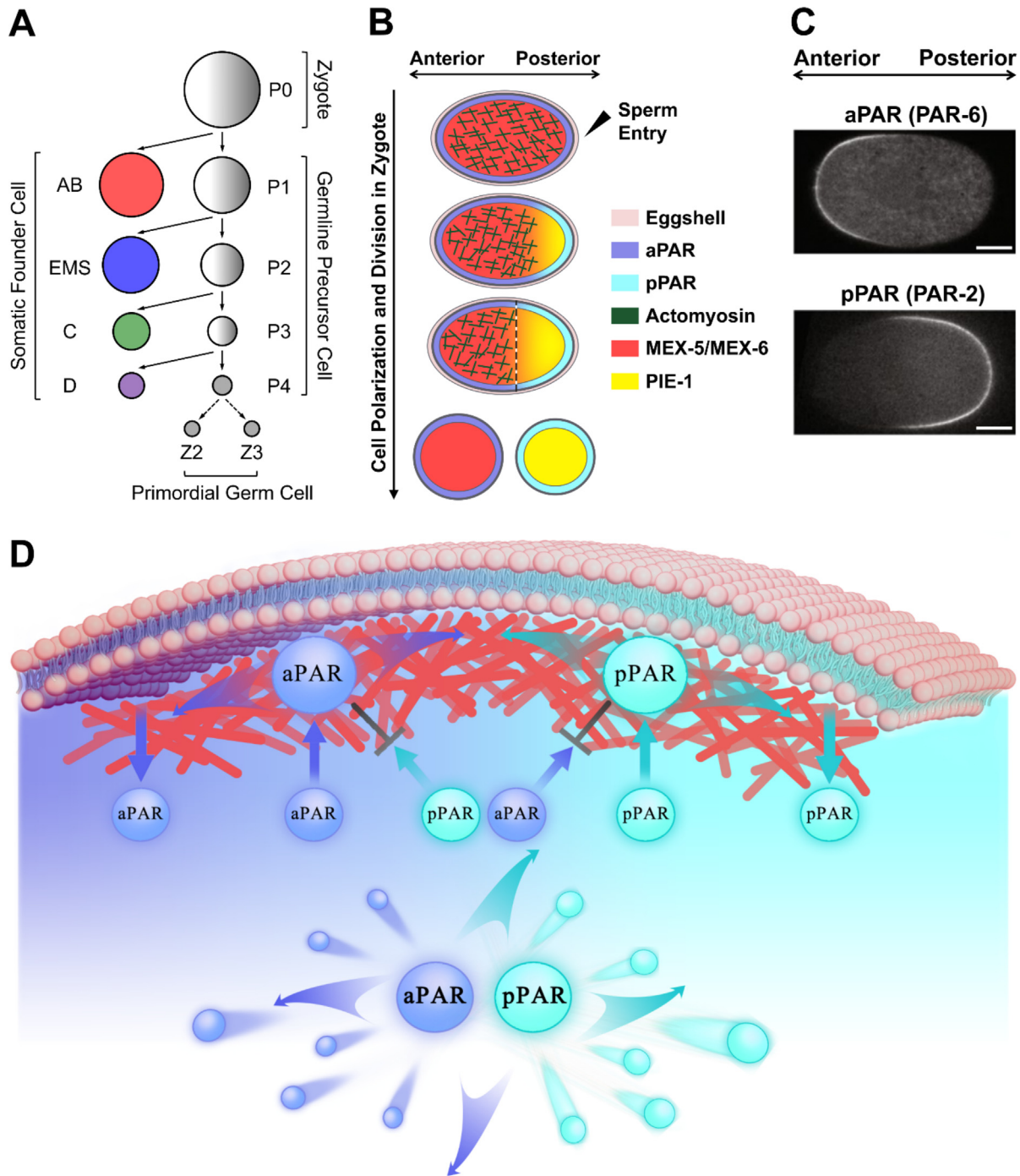


**Fig. 2.** Polarization of zygote and germline precursor cells and specification of somatic founder cells in early embryogenesis of *C. elegans*. (A) Consecutive asymmetric divisions from P0 to P3 that sequentially generate somatic founder cells (AB, EMS, C, and D) and symmetric division in P4 that ultimately generates primordial germ cells (Z2 and Z3). (B) Polarization of upstream aPAR and pPAR (shown with distributions on the membrane) and downstream MEX-5/MEX-6 and PIE-1 (shown with distributions in the cytosol) in P0 that is induced by sperm entry. The actomyosin meshwork that flows from the posterior to the anterior in P0 and drives the initial regionalization of aPAR is depicted as thin lines. The color of each component is listed on the right. The stable final boundary between the anterior and the posterior in P0 is represented by a dashed line that splits the zygote into two future daughter cells (the larger cell = the somatic founder cell AB; the smaller cell = the germline precursor cell P1). This schematic is adapted from [174]. (C) Fluorescent labeling of aPAR and pPAR, exemplified by PAR-6 and PAR-2, respectively; both images are reproduced from [163] with permission. A bar representing an actual length of 10  $\mu\text{m}$  is depicted in the bottom-right corner of each experimental image. (D) Schematic showing the migration of aPAR (blue) and pPAR (cyan) between the membrane and the cytosol (straight arrows). Their diffusion and mutual inhibition are indicated by curved and gray blunt-ended arrows, respectively, while the red rods represent the cell cortex. (For interpretation of the references to color in this figure legend, the reader is referred to the web version of this article.)

lished in P0 and is triggered by the entry of sperm, with the entry site determining the posterior of the embryo (Fig. 2B) [164]. Two groups of membrane-bound partitioning-defective (PAR) proteins generate cell polarity by mutually inhibiting their membrane asso-

ciation and thus localize on opposite sides of a cell (Fig. 2C and 2D). At the 1-cell stage, the embryo is embedded in an ellipsoidal eggshell whose major axis becomes the anterior–posterior (a–p) axis of the embryo by polarization, and the PAR proteins in the a and



p regions are therefore named aPAR (PAR-3, PAR-6, and PKC-3) and pPAR (PAR-1 and PAR-2) [165]. The localization of PAR proteins conveys positional information to their downstream molecules, such as MEX-5/MEX-6, PIE-1, and P granule, which are thus polarized and spatially separated [159]. Additionally, a few molecules, such as actomyosin, CDC-42, CHIN-1, and possibly some downstream molecules (e.g., MEX-5/MEX-6), are involved in the interaction network and cortical activity that facilitate cell polarization [17,166,167].

A key aim of systems biology is to integrate mathematical and physical approaches with biological knowledge to interpret how genetic circuits determine the dynamics and function of a network system, as this enables the delineation of biological mechanisms and establishes a sound foundation for synthetic biological studies [168–172]. The determination that aPAR and pPAR shuttle between the membrane and the cytosol, diffuse, and interact with each other provides a good basis for such studies [173]. Many auxiliary molecular interactions (motifs) and coupling mechanisms (such as advective transport in the cortex) can be exploited for characterizing the delicate control of cell-polarization patterning and its underlying design principles [174].

### 3.1.2. Critical role of the mutual inhibition of aPAR and pPAR

The knowledge obtained from empirical studies of P0–P4 has allowed mathematical and physical modeling-based investigations of the theoretical principle of cell polarization in *C. elegans*. Tostevin *et al.* (2008) introduced one-dimensional reaction–diffusion equations to model the distributions of aPAR and pPAR in the cortex and cytosol of *C. elegans* zygote, based on which they suggested that these proteins' simple mutual inhibition is sufficient to generate their anterior–posterior domain separation [175]. In a comprehensive computational study of protein network circuits capable of cell polarization, Chau *et al.* (2012) showed that mutual inhibition is a core mechanism in such circuits [172]. Using a combination of computational and experimental techniques, Goehring *et al.* (2011) demonstrated that the advective flow of actomyosin in the cortex of *C. elegans* zygote is a critical trigger and facilitator of the robust segregation of PAR proteins and established a mechanochemical scheme for cell polarization [176,177]. In other research, Kravtsova *et al.* (2014) provided theoretical evidence that actomyosin contractility is required to stabilize the polarity pattern and that this mechanical cue can only break cell symmetry in the presence of certain chemical interactions [178]. Seirin-Lee *et al.* (2015) examined the morphometric features of the polarity distribution and found that polarity proteins' advective transport in the membrane and cytosol and their mass concentrations in these regions regulate the width of the posterior domain [179]. Seirin-Lee *et al.* (2020) also mathematically and numerically explored the polarity distribution from upstream to downstream molecules (i.e., from PARs to MEX-5/MEX-6 to PIE-1) [180]. Gross *et al.* (2019) probed how guiding cues and biochemical feedback affect *C. elegans* cell polarization and manifest a transition point where the system changes from a guide-dominated to a feedback-dominated state [181]. In addition to the explorations of the *C. elegans* 1-cell embryo, Lim *et al.* (2021) used computational modeling, fluorescent imaging, and genetic perturbation to scrutinize the differentiated *C. elegans* 2-cell embryo, which revealed that the balance of the most upstream PAR proteins independently determines whether the symmetric or asymmetric mode of division occurs [182].

The effect of geometric cues on cell polarization is also a popular research theme. Dawes *et al.* (2013) used a reaction–diffusion model and an Allen–Cahn equation in two-dimensional space to elucidate that the cortical thickness distribution can determine the position of the interface between the exclusive domains of aPAR and pPAR [183]. Aras *et al.* (2018) used a phase field model to simulate the actomyosin contraction dynamics during the first

cell polarization and division in the *C. elegans* embryo; this revealed that the rigid eggshell of the embryo generates asymmetric cortical tension that restricts changes in cell shape and consequently affects cell morphology and the timing of polarity establishment [184]. Another study, Geßele *et al.* (2020), found that the local ratio of membrane-surface-to-cytosolic-volume, which is high at the two terminals of an embryo and low in the middle of an embryo, plays an important role in the formation of polarity by mediating protein shuffling between the membrane and the cytosol [185]. The cell size was also determined to be crucial for the establishment of polarity, due to the reaction–diffusion system describing the interplay between aPAR and pPAR not being linearly scalable; this explains why the asymmetric division doesn't take place in the last germline precursor cell, P4 [163]. In theory, the location of the transition region between anterior and posterior domains is sensitive to changes in cell shape when a cell is relatively small, which implies that additional programmed regulation might be employed to ensure the precision and robustness of cell polarization [186].

### 3.1.3. Investigation of additional motifs and regulations

In addition to the mutual inhibition exhibited by PAR proteins, other proteins and their interactions and feedback have been extensively investigated using theoretical methods. Dawes *et al.* (2011) studied the self-association of aPAR, which is realized by PAR-3 oligomerization, and proved that it functions in establishing and stabilizing polarity regardless of cortical activity [187]. In another work, Seirin-Lee *et al.* (2020), minimal network analysis and eFAST sensitivity analysis revealed that the active regulation of aPAR by CDC-42 helps maintain the anterior and posterior polarity domains and polarization itself [188]. Given the fact that the depletion of the downstream protein MEX-5/MEX-6 is harmful to the polarity of upstream PAR proteins in later germline precursor cells, Seirin-Lee (2021) hypothesized their inhibitive regulation on aPAR's association on membrane and active regulation on aPAR's dissociation from membrane; computation showed that both two assumed loops can reinforce PAR polarity [17,167,189]. Further research on cell polarization in P2, which has the opposite polarity to its ancestors P1 and P0 *in vivo*, showed that the above-mentioned effect was due to the contact-based MES-1/SRC-1 signaling from P2's sister cell, EMS, that enhances the on-rate of PAR-2 [190].

Overall, these above-described theoretical explorations have delineated crucial aspects of the diverse and precise control of cell polarization in *C. elegans*. These programs give rise to the stereotypical development of *C. elegans* embryos and are vital for optimal cell proliferation, morphogenesis, and differentiation [92,160,191]. Other experimental observations, such as that the LGL-1 is localized in the posterior of *C. elegans*, can be included to form a complete interaction network for future studies [191].

## 3.2. Mechanical modeling of cell positioning and cell morphology

Many mechanical models have been used to investigate embryonic morphogenesis in various species. As the early development of *C. elegans* is highly precise and repeatable in individual embryos, for the past two decades researchers have attempted to reproduce the progression of its cellular arrangement *in silico*.

### 3.2.1. Multi-particle model

In 2003, Kajita *et al.* reported their physical model that describes the cell shape and the intercellular and intracellular mechanical interactions in the early embryo of *C. elegans* (Fig. 3A) [192]. In this model, multiple particles with a certain mass are used to represent various subcellular structures; for example, (1) the cell membrane consists of particles that interact with each

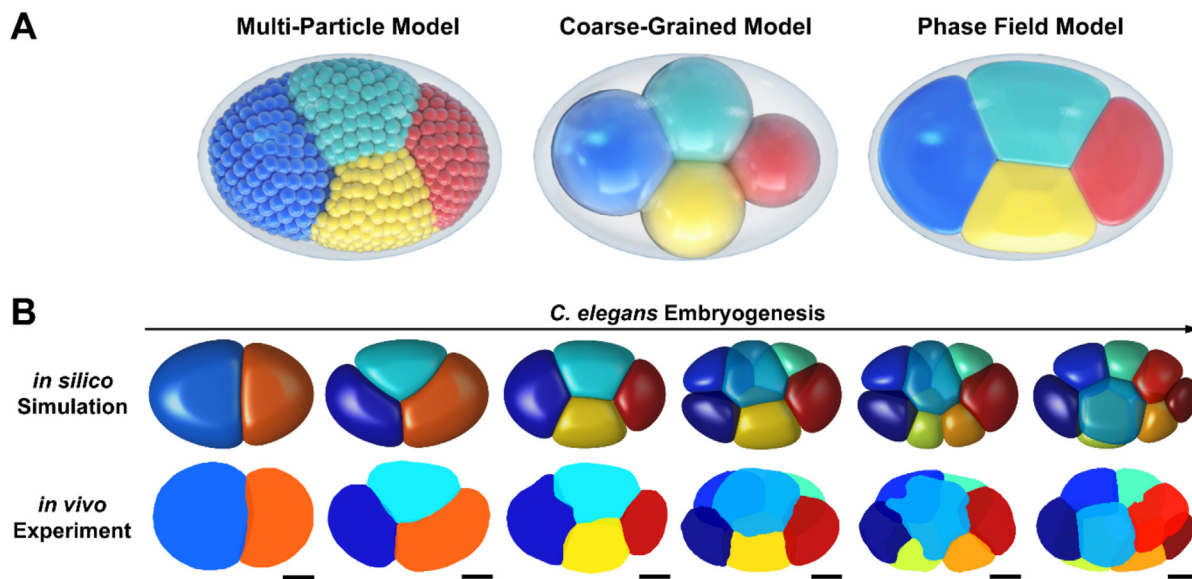


**Fig. 3.** Mechanical modeling of cell positioning and cell morphology in *C. elegans* embryogenesis. (A) Schematic diagrams of the multi-particle model (left), the coarse-grained model (middle), and the phase field model (right) at the 4-cell stage. (B) Embryonic morphologies acquired from *in silico* simulation by the phase field model (first row) and *in vivo* experiment (second row) from the 2- to 8-cell stages. The subfigures of *in silico* embryonic morphologies are reproduced from [57], and the *in vivo* embryonic morphologies with their segmentation outputs are rendered by CShaper, with a scale bar representing an actual length of 10  $\mu\text{m}$  depicted beneath each [76].

other via a spring and damper; (2) these membrane particles are assigned an inner pressure and bending force to control the cell size and cell shape, respectively; and (3) the membrane particles are supported by a centrosome, which serves as the cell center and can model cell division by separating into two distant and mutually repulsive centrosomes. This model was shown to reconstruct cell shape dynamics for 1- to 4-cell morphogenesis restricted by an ellipsoidal eggshell that were similar to real dynamics and to classify four different shapes of embryonic structures (i.e., diamond-, parallelogram-, square-, and T-shaped structures) as its mechanical parameters are varied. Further analysis revealed that the forces between centrosomes and between the membrane and the centrosome during cytokinesis are important for the generation of the diamond-shaped structure seen *in vivo*, while the maximum distance between centrosomes directly controls cell elongation and skewing and is therefore the primary factor determining cell patterning.

Kajita *et al.* noted key differences between the cell shapes generated by their model and those observed in experiments and thus developed a better model that simulates the rounding and stiffening during cell division [193]. This is realized by reinforcing the repulsion between membrane particles and between the membrane and the centrosome and the bending force of the membrane, which reproduces the curved interface between AB and P1 at the end of the 2-cell stage (i.e., where AB is protruding toward P1). The researchers optimized the mechanical parameters by examining how frequently the model generates the diamond-shaped structure, which revealed that both cell rounding and cell stiffening affect the *in silico* pattern formation. However, tests demonstrated that cell stiffening is more important than cell rounding in the model. The advantage of the multi-particle model is its ability to describe subcellular components (e.g., the membrane, centrosome, and contractile ring) in sufficient detail to reproduce cell morphology. However, the approximately 20 parameters of the model that have biological significance are difficult to measure or fit experimentally, which limits further application of the model.

### 3.2.2. Coarse-grained model

The coarse-grained model simplifies a cell by representing it as a single point, with the interaction (e.g., repulsion and attraction)

between cells being pairwise and distance-dependent, so it incurs low computational costs (Fig. 3A). As this model has minimal parameters it can reveal some fundamental rules of a mechanical system. In 2013, Fickentscher *et al.* adopted the coarse-grained model to determine whether cell arrangement patterns are primarily an outcome of mechanical interaction and relaxation [194]. In their form of the model, the cells are treated as repellent elastic balls enveloped by an ellipsoidal eggshell and governed by Langevin equations with random noise, and cell division and cell adhesion are not considered. Surprisingly, the simulated close-packing configurations at the 4-, 8-, and 12-cell stages are within the natural range measured by imaging cell nucleus positions via light-sheet microscopy, indicating the role of mechanical cues in determining cell arrangement. Furthermore, they found that the formation of the planar diamond-shaped pattern at the 4-cell stage, in which the dorsal–ventral axis is established, is primarily controlled by repulsive force exerted by the eggshell. Fickentscher *et al.* (2016) then incorporated cell division into their model and also asked “how do individual cells know that dividing right now is a good choice for a meaningful and robust mechanically driven arrangement of all cells in the embryo?” [90]. They concluded in this and another study that the experimentally observed anticorrelation between cell cycle length ( $T$ ) and cell volume ( $V$ ) is significant and lineage-specific [90,91]. After experimentally fitting the formulated  $T$ – $V$  relationship, they found that a simulation of the cell arrangement at the 24-cell stage (i.e., prior to the onset of gastrulation) resembles the *in vivo* situation. Their simulations with a range of values of parameters suggest that programmed cell-division asymmetry provides sufficient time for cells to relax into their required positions after cell division. Moreover, as the number of cells increases and their size decreases as embryogenesis advances, the system becomes more sensitive to local perturbations and thus more prone to producing irrecoverable defects.

Tian *et al.* (2020) concentrated on the cell division sequence that is highly conserved between *C. elegans* embryos and other *Caenorhabditis* species and showed that both the interval of relaxation and the order of cell division events must be controlled for the correct cell arrangement pattern to be generated [72,73,75,195]. In addition, they found that the synchrony of cell divisions is programmed in a particular manner to ensure that cells

move collectively, so that cell arrangement patterns do not bifurcate. Moreover, they determined that the cell division orientation known to be regulated by cell–cell contact geometry and cell–cell signaling is important for generating the stereotypical cell arrangement pattern *in vivo*.

In summary, the above-described theoretical studies using coarse-grained models have highlighted that cell division is carefully programmed to ensure that there is a precise and robust progression of cell arrangement during *C. elegans* embryogenesis.

The coarse-grained model has also been applied to study specific biological phenomena. In 2017, Yamamoto *et al.* reported that the RNAi knockdown of the genes *dpy-1* and *lon-1* generated *C. elegans* eggshells with variable aspect ratios, in which at the 4-cell stage they identified a variety of cell arrangement patterns (i.e., diamond, pyramid, T-shaped, and linear patterns) [196]. The distribution of cell arrangement patterns with respect to aspect ratio cannot be reproduced by a coarse-grained model that considers only cell–cell repulsion but can be reproduced by the improved coarse-grained model that considers cell–cell attraction in addition to cell–cell repulsion [90,194,196]. Fluorescence imaging of the cell adhesive protein HMR-1 showed that it accumulates in significantly lower amounts at the interface between EMS and P2 than at the interface between other cells, and the improved model—which incorporates this in the form of an asymmetric adhesion map—captures the empirical distribution of cell arrangement patterns [196]. Moreover, the RNAi-mediated elimination of cell adhesion generates a different distribution of cell arrangement patterns, confirming the role of a cell–cell adhesion map in determining the cell arrangement pattern. Another study revealed that microinjecting an actin inhibitor into the AB cell to interfere with its adhesion function effectively increased the level of HMR-1 accumulation at the EMS–P2 interface, suggesting that a cell–non-autonomous mechanism programs the distribution of cell–cell adhesion [197]. Therefore, it appears that mechanical interaction (e.g., cell adhesion) and spatial confinement serve as key regulatory factors that specify the cell arrangement pattern in the *C. elegans* 4-cell embryo [198,199].

Recently, Miao *et al.* (2022) applied a coarse-grained model that considers both intercellular repulsion and attraction and used experimentally measured cell-division order and volume segregation ratio as inputs to simulate cell division and motion up to the ~ 330-cell stage of *C. elegans* [75,76,200]. These studies have shown that even though the orientation of each cell division is set to be nearly tangential to the eggshell, cell internalization occurs spontaneously in all conditions and mimics the behavior of gastrulation, during which a cell originally in contact with the eggshell moves inward the embryo such that the cell becomes surrounded by other cells. The researchers have also found that the lateral compression and pressure between cells becomes increasingly stronger because of the reduction in cell size during proliferation, and that the internalization of a cell effectively decreases such stress and lowers the potential energy of the entire system. Moreover, they have used force analysis and numerical simulation to predict that bistable states exist during the 15- to 44-cell stages and that a larger cell has a stronger tendency to internalize than a smaller cell. In the real *C. elegans* embryo, the gut precursor cells E2 (Ea and Ep) become the largest of all cells in the embryo due to the initiation of tissue-specific zygotic transcription and consequent lengthened cell cycle and gastrulate during the 26- to 44-cell stages, which is very close to the theoretically predicted one [46,117]. Furthermore, systematic virtual experiments using the coarse-grained model showed how boundary geometry, cellular mechanical properties such as stiffness and adhesion, and cell-specific active regulation affect cell internalization [200].

Overall, studies of embryonic morphogenesis at the 4-cell and gastrulation stages have suggested that a simple coarse-grained model can recapitulate the fundamental features of the embryonic

system of *C. elegans*, thereby enabling the design and optimization strategy of the genetic programs to be rationally interpreted.

In 2020, Guan *et al.* revised the coarse-grained model by optimizing the formulation and parameters and inputting experimentally measured cell volumes and eggshell shape to determine the latest developmental stage to which it can be applied with sufficient precision [76,201]. They found that the model can reproduce cell positions up to the 26-cell stage (at which time they are assumed to be at mechanical equilibrium) with positional variation that is less than a cell's radius for all cells. Moreover, they determined that the model performs well even at the 51-cell stage, except for three cells that exhibit a deviation larger than their radii, suggesting that the system at this stage remains largely governed by mechanical cues but that additional modifications (e.g., inhomogeneous cell stiffness and cell adhesion) might have a non-negligible effect on some cells. In addition, these researchers found that the cell–cell contact relationship conserved among embryos is poorly reproduced by the coarse-grained model, although the inclusion of a heterogeneous cell–cell adhesion map derived from cell–cell contact data somewhat improves the reconstruction performance of the model [201].

The limitation of the coarse-grained model was also discussed by Yamamoto *et al.* (2017) in light of its failure to reproduce the T-reverse-type pattern in an elongated eggshell with depleted cell adhesion [196]. The discrepancy between coarse-grained simulations and experiments is not surprising, given that the model oversimplifies each cell (i.e., as a single point) and therefore does not include information on cell morphology. Models with higher complexity (e.g., the multi-particle model and the phase field model) are needed to answer questions on cell morphology and more complex cellular properties.

### 3.2.3. Phase field model

The phase field model, which was originally developed in materials science to describe the concentration, interaction, and separation of multiple components, uses a diffusible scalar (phase) field to represent an object and track its interfacial interactions with other objects (Fig. 3A) [202–205]. In the past two decades, this approach has been used in cell modeling, wherein a cell is treated as a 2D or 3D field and thus has interfacial interactions with other cells and with an external boundary, and the shape of a cell is programmable to determine its response to mechanical and biochemical stimuli [206,207]. Recently, this approach has been applied to examine *C. elegans* embryonic morphogenesis.

In 2019, Jiang *et al.* reported a phase field model for simulating cell growth, cell division, cell–cell contact, and the mechanical moduli of a cell and modeled cell compaction and packing under soft constraints [208]. They tested the model in two dimensions and found that it generates cell morphologies and positions that are similar to those experimentally observed in the *C. elegans* embryo. Kuang *et al.* (2022) utilized the 3D time-lapse cell morphology data of the CShaper system to construct a more sophisticated 3D phase field model that takes into account cell surface tension, cell–eggshell and cell–cell repulsion, cell–cell attraction, and cell volume constriction [57,76]. They showed that by inputting *in vivo* data of cell-division order, orientation, and volume segregation ratio into the model and performing step-by-step model construction and verification, the model accurately reconstructs cell morphology and the conserved cell–cell contact map (Fig. 3B). Furthermore, they found that the cell adhesion program can be inferred without *a priori* knowledge by comparison of the simulated morphologies with the experimentally observed morphologies [196,209]. The model is also able to characterize the *in vivo* system in space and time, such that it can account for the timing and orientation of cell division and the cell–cell attraction matrix programmed from the 6- to 8-cell stages. However, despite

the outstanding accuracy of the phase field model, high computational time and memory costs are incurred during its computation of the partial differential equation and the dense grid, which hamper its further application. Accordingly, the phase-field framework was recently upgraded by resolution refinement, formula optimization, and numerical scheme improvement, which enables it to compute over 100 cells with considerable efficiency and accuracy [210].

The phase-field method has also been applied to solve the problem of *T*-reversed-type cell arrangement at the 4-cell stage, which was observed in a genetically perturbed egg with a high aspect ratio and weak/no cell adhesion, and which cannot be reproduced by a coarse-grained model [196,211]. Seirin-Lee *et al.* (2022) used a 2D phase field model and real eggshell morphologies extracted from experimental images to reproduce the *T*-reversed-type pattern under a condition with experimental parameters [211]. They assigned an ellipsoid and a capsule eggshell with the same aspect ratio in the simulation and found that the capsule eggshell, which is more similar than the ellipsoid eggshell to the real eggshell in a *T*-reversed-type embryo, leaves more extra-embryonic space for cell movement. This was verified by experimental data, establishing that this extra-embryonic space is another geometric factor that modulates the cell arrangement in concert with mechanical parameters, such as cell stiffness and cell adhesion.

In summary, the quantitative morphology data obtained from the above-described studies have effectively guided the development of comprehensive mechanical models that serve as ground truth. This has deepened our understanding of the *in vivo* developmental system of *C. elegans* and enhanced our ability to predict its behavior.

#### 4. Summary and outlook

Rapid technological advancements in live-cell imaging allow rapid acquisition of high-resolution images of molecular and cellular events throughout development. Thus, what scientific questions can or should we ask and what roles can computational modeling play in this regard? Developmental biologists have delineated the developmental patterns of *C. elegans* and uncovered details of its developmental processes and regulatory mechanisms by direct observation and/or genetic perturbation experiments. These explorations have mainly been conducted using genetic approaches, such as the identification of stepwise Wnt and Notch signaling events between specific interacting cell pairs [19–24,26,93]. These have been followed by more systems-level studies, aided by 4D live-cell imaging data, which have taken into account all of the cells derived from different lineages with different fates and have accurately measured the positioning and division timing and orientation of each cell throughout embryogenesis [13,54–56]. This quantitative single-cell-resolution 4D data and the stereotypical procedures of *C. elegans* embryogenesis have drawn the attention of mathematicians and physicists, who have attempted to provide theoretical explanations for various observations, such as why the developmental program has the design. For instance, in modeling cell positioning, physical simulations show why the timing and orientation of cell division and cell–cell adhesion are programmed as they are *in vivo* [57,90,195,196]. In mechanical terms, this programming ensures the precise and robust realization of the developmental path of embryonic morphology [19,20,75,89,91–95,197,209,212]. Physical modeling also provides answers to the perennial question of why and how the *C. elegans* developmental procedure is so reproducible. However, there remains a large gap between data and theory, as there are much more data than theory and modeling can absorb, interpret, and exploit. Accordingly, there is a need for

more theorists to be involved in studies to assist in the interpretation of high-quality quantitative data. Seamless collaboration between experimentalists and theorists will be crucial for developing a deep understanding of the embryogenesis program from both genetic and physical perspectives by making full use of data and models.

Reliable quantitative data serve as ground truth to verify or falsify theoretical and computational models. The physicist Richard Feynman wrote on his blackboard “what I cannot create, I do not understand”; similarly, reconstituting a biological process *in silico* is a way to test how well the process is understood [213]. The increasing amount of data on *C. elegans* embryogenesis will greatly aid the construction of accurate theories, algorithms, and mathematical language to describe this organism’s development. Conversely, theoretical endeavors will stimulate new experiments, new applications of technologies, and the generation of new data. For example, the *in situ* measurement of cell mechanical properties (e.g., cell–cell adhesion mediated by HMR-1) is extremely difficult to perform when the signal-to-noise ratio of fluorescence drastically decays during blastomere cleavage [196,209]. This impedes accurate modeling, especially of developmental stages with dozens to hundreds of cells [57,201]. This problem also occurs in the reconstruction of cell morphology from imaging data beyond the 350-cell stage [76]. For these and other reasons, we believe that in many cases the advancement of data generation and theory should be complementary and mutually stimulating.

The interaction and integration of quantitative data and modeling are essential to answer two key questions that have been posed by the developmental biologist Lewis Wolpert: “Will the egg be computable?” and “Do we understand development?” [214,215]. These questions are related but not the same. On the one hand, even if egg development could be perfectly simulated *in silico*, it is not guaranteed that this would inevitably result in a comprehensive understanding of the process. This is analogous to the fact that simulating the exact trajectory of all of the air molecules in a room would not necessarily result in an understanding of thermodynamics. On the other hand, it is possible that a certain level of understanding can be achieved without detailed and “realistic” modeling (again, the example of thermodynamics). Thus, the answer to one question would help to answer the other question, and *vice versa*. Overall, models aid understanding, and models of different scales and complexity are needed to answer different questions.

#### Funding

This work was supported by funding from the National Natural Science Foundation of China (Grant No 12090053 and 32088101) to G. Guan and C. Tang and from the Hong Kong Research Grants Council (Grant No HKBU12101520, HKBU12101522, N\_HKBU201/18, and FNRA-IG/21–22/SCL\_02) to Z. Zhao.

#### Declaration of Competing Interest

The authors declare that they have no known competing financial interests or personal relationships that could have appeared to influence the work reported in this paper.

#### Acknowledgments

We thank all members of the Tang Lab and the Zhao Lab for their constructive comments and Xiangyu Kuang and Yixuan Chen for helpful discussions and diagram presentations. We are also grateful to Prof. Feng Liu and Prof. Peng Xia for their professional advice on the summary of advanced experimental biotechnology.

Our gratitude is also extended to Kai Kang for his assistance in data visualization.

## References

- [1] Byerly L, Cassada RC, Russell RL. The life cycle of the nematode *Caenorhabditis elegans*. I. Wild-type growth and reproduction. *Dev Biol* 1976;51(1):23–33.
- [2] Riddle DL, Blumenthal T, Meyer BJ, Priess JR. *C. elegans* II. 2nd edition. Cold Spring Harbor Laboratory Press; 1997.
- [3] Soete G, Betist MC, Korswagen HC. Regulation of *Caenorhabditis elegans* body size and male tail development by the novel gene *lon-8*. *BMC Dev Biol* 2007;7:20.
- [4] Ha NM, Tran SH, Shim Y-H, Kang K. *Caenorhabditis elegans* as a powerful tool in natural product bioactivity research. *Appl Biol Chem* 2022;65:18.
- [5] Martini E. Die Zellkonstanz und ihre Beziehungen zu anderen zoologischen Vorwürfen. *Zeit Anat Entwickl* 1923;70:179–259.
- [6] van Cleave HJ. Eutely or cell constancy in its relation to body size. *Q Rev Biol* 1932;7(1):59–67.
- [7] Kenyon C. Cell lineage and the control of *Caenorhabditis elegans* development. *Philos Trans R Soc Lond B Biol Sci* 1985;312(1153):21–38.
- [8] Sulston JE. Post-embryonic development in the ventral cord of *Caenorhabditis elegans*. *Philos Trans R Soc Lond B Biol Sci* 1976;275(938):287–97.
- [9] Sulston JE, Horvitz HR. Post-embryonic cell lineages of the nematode, *Caenorhabditis elegans*. *Dev Biol* 1977;56(1):110–56.
- [10] Deppe U, Schierenberg E, Cole T, Krieg C, Schmitt D, Yoder B, et al. Cell lineages of the embryo of the nematode *Caenorhabditis elegans*. *Proc Natl Acad Sci U S A* 1978;75(1):376–80.
- [11] Kimble J, Hirsh D. The postembryonic cell lineages of the hermaphrodite and male gonads in *Caenorhabditis elegans*. *Dev Biol* 1979;70(2):396–417.
- [12] Sulston JE, Schierenberg E, White JG, Thomson JN. The embryonic cell lineage of the nematode *Caenorhabditis elegans*. *Dev Biol* 1983;100(1):64–119.
- [13] Schnabel R, Hutter H, Moerman D, Schnabel H. Assessing normal embryogenesis in *Caenorhabditis elegans* using a 4D microscope: Variability of development and regional specification. *Dev Biol* 1997;184(2):234–65.
- [14] Richards JL, Zacharias AL, Walton T, Burdick JT, Murray JI. A quantitative model of normal *Caenorhabditis elegans* embryogenesis and its disruption after stress. *Dev Biol* 2013;374(1):12–23.
- [15] Ho VWS, Wong M-K, An X, Guan D, Shao J, Ng HCK, et al. Systems-level quantification of division timing reveals a common genetic architecture controlling asynchrony and fate asymmetry. *Mol Syst Biol* 2015;11(6):814.
- [16] Hubbard EJA, Greenstein D. Introduction to the germ line. *WormBook* 2005.
- [17] Schubert CM, Lin R, de Vries CJ, Plasterk RHA, Priess JR. MEX-5 and MEX-6 function to establish soma/germline asymmetry in early *C. elegans* embryos. *Mol Cell* 2000;5(4):671–82.
- [18] Gangshetti U, Kelly WG. Establishment and maintenance of heritable chromatin in *C. elegans*. *JSM Genet Genomics* 2017;4(1):1022.
- [19] Thorpe CJ, Schlesinger A, Carter JC, Bowerman B. Wnt signaling polarizes an early *C. elegans* blastomere to distinguish endoderm from mesoderm. *Cell* 1997;90(4):695–705.
- [20] Rocheleau CE, Downs WD, Lin R, Wittmann C, Bei Y, Cha YH, et al. Wnt signaling and an APC-related gene specify endoderm in early *C. elegans* embryos. *Cell* 1997;90(4):707–16.
- [21] Zacharias AL, Walton T, Preston E, Murray JI. Quantitative differences in nuclear  $\beta$ -catenin and TCF pattern embryonic cells in *C. elegans*. *PLoS Genet* 2015;11(10):e1005585.
- [22] Mello CC, Draper BW, Priess JR. The maternal genes *apx-1* and *glp-1* and establishment of dorsal-ventral polarity in the early *C. elegans* embryo. *Cell* 1994;77(1):95–106.
- [23] Hutter H, Schnabel R. *glp-1* and inductions establishing embryonic axes in *C. elegans*. *Development* 1994;120(7):2051–64.
- [24] Mango SE, Thorpe CJ, Martin PR, Chamberlain SH, Bowerman B. Two maternal genes, *apx-1* and *pie-1*, are required to distinguish the fates of equivalent blastomeres in the early *Caenorhabditis elegans* embryo. *Development* 1994;120(8):2305–15.
- [25] Lee J-Y, Marston DJ, Walston T, Hardin J, Halberstadt A, Goldstein B. Wnt/ Frizzled signaling controls *C. elegans* gastrulation by activating actomyosin contractility. *Curr Biol* 2006;16(20):1986–97.
- [26] Moskowitz IP, Rothman JH. *lin-12* and *glp-1* are required zygotically for early embryonic cellular interactions and are regulated by maternal GLP-1 signaling in *Caenorhabditis elegans*. *Development* 1996;122(12):4105–17.
- [27] Brenner S. The genetics of behaviour. *Br Med Bull* 1973;29(3):269–71.
- [28] Brenner S. The genetics of *Caenorhabditis elegans*. *Genetics* 1974;77(1):71–94.
- [29] Sulston JE, Brenner S. The DNA of *Caenorhabditis elegans*. *Genetics* 1974;77(1):95–104.
- [30] *C. elegans* Sequencing Consortium. Genome sequence of the nematode *C. elegans*: A platform for investigating biology. *Science* 1998;282(5396):2012–8.
- [31] International Human Genome Sequencing Consortium. Initial sequencing and analysis of the human genome. *Nature* 2001;409:860–921. <https://www.nature.com/articles/35057062>
- [32] Stein LD, Bao Z, Blasiar D, Blumenthal T, Brent MR, Chen N, et al. The genome sequence of *Caenorhabditis briggsae*: A platform for comparative genomics. *PLoS Biol* 2003;1(2):e45.
- [33] Hillier LW, Coulson A, Murray JI, Bao Z, Sulston JE, Waterston RH. Genomics in *C. elegans*: So many genes, such a little worm. *Genome Res* 2005;15(12):1651–60.
- [34] Lee R. Web resources for *C. elegans* studies. *WormBook* 2005.
- [35] Davis P, Zarowiecki M, Arnaboldi V, Becerra A, Cain S, Chan J, et al. *WormBase* in 2022 - Data, processes, and tools for analyzing *Caenorhabditis elegans*. *Genetics* 2022;220(4):iyac003.
- [36] Meneely PM, Dahlberg CL, Rose JK. Working with worms: *Caenorhabditis elegans* as a model organism. *Curr Protoc Essent Lab Tech* 2019;19:e35.
- [37] The Nobel Prize. <https://www.nobelprize.org/prizes/lists/all-nobel-prizes>.
- [38] Ellis HM, Horvitz HR. Genetic control of programmed cell death in the nematode *C. elegans*. *Cell* 1986;44(6):817–29.
- [39] Ellis RE, Horvitz HR. Two *C. elegans* genes control the programmed deaths of specific cells in the pharynx. *Development* 1991;112(2):591–603.
- [40] Hengartner MO, Ellis RE, Horvitz HR. *Caenorhabditis elegans* gene *ced-9* protects cells from programmed cell death. *Nature* 1992;356:494–9.
- [41] Ellis RE, Jacobson DM, Horvitz HR. Genes required for the engulfment of cell corpses during programmed cell death in *Caenorhabditis elegans*. *Genetics* 1991;129(1):79–94.
- [42] Fire A, Xu S, Montgomery MK, Kostas SA, Driver SE, Mello CC. Potent and specific genetic interference by double-stranded RNA in *Caenorhabditis elegans*. *Nature* 1998;391:806–11.
- [43] Conte DJ, MacNeil LT, Walhout AJM, Mello CC. RNA interference in *Caenorhabditis elegans*. *Curr Protoc Mol Biol* 2015;109:26.3.1–26.3.30.
- [44] Du Z, Santella A, He F, Shah PK, Kamikawa Y, Bao Z. The regulatory landscape of lineage differentiation in a metazoan embryo. *Dev Cell* 2015;34(5):592–607.
- [45] Santella A, Kovacevic I, Herndon LA, Hall DH, Du Z, Bao Z. Digital development: A database of cell lineage differentiation in *C. elegans* with lineage phenotypes, cell-specific gene functions and a multiscale model. *Nucleic Acids Res* 2016;44(D1):D781–5.
- [46] Wong M-K, Guan D, Ng KHC, Ho VWS, An X, Li R, et al. Timing of tissue-specific cell division requires a differential onset of zygotic transcription during metazoan embryogenesis. *J Biol Chem* 2016;291(24):12501–13.
- [47] Chalfie M, Tu Y, Euskirchen G, Ward WW, Prasher DC. Green fluorescent protein as a marker for gene expression. *Science* 1994;263(5148):802–5.
- [48] Boveri T. Über die Entstehung des Gegensatzes zwischen den Geschlechtszellen und den somatischen Zellen bei *Ascaris megalocephala*, nebst Bemerkungen zur Entwicklungsgeschichte der Nematoden. *Sitzungsber Ges Morph Physiol München* 1892;8:114–25.
- [49] Goldschmidt RB. Das Nervensystem von *Ascaris lumbricoides* und *megalcephala*. *I. Z Wiss Zool* 1908;90:73–136.
- [50] Goldschmidt RB. Das Nervensystem von *Ascaris lumbricoides* und *megalcephala*. *II. Z Wiss Zool* 1909;92:306–57.
- [51] Hird SN, White JG. Cortical and cytoplasmic flow polarity in early embryonic cells of *Caenorhabditis elegans*. *J Cell Biol* 1993;121(6):1343–55.
- [52] Schnabel R, Bischoff M, Hintze A, Schulz A-K, Hejnal A, Meinhardt H, et al. Global cell sorting in the *C. elegans* embryo defines a new mechanism for pattern formation. *Dev Biol* 2006;294(2):418–31.
- [53] Bischoff M, Schnabel R. Global cell sorting is mediated by local cell-cell interactions in the *C. elegans* embryo. *Dev Biol* 2006;294(2):432–44.
- [54] Bao Z, Murray JI, Boyle T, Ooi SL, Sandel MJ, Waterston RH. Automated cell lineage tracing in *Caenorhabditis elegans*. *Proc Natl Acad Sci U S A* 2006;103(8):2707–12.
- [55] Murray JI, Bao Z, Boyle TJ, Waterston RH. The lineaging of fluorescently-labeled *Caenorhabditis elegans* embryos with StarryNite and AceTree. *Nat Protoc* 2006;1(3):1468–76.
- [56] Boyle TJ, Bao Z, Murray JI, Araya CL, Waterston RH. AceTree: A tool for visual analysis of *Caenorhabditis elegans* embryogenesis. *BMC Bioinform* 2006;7:275.
- [57] Kuang X, Guan G, Wong M-K, Chan L-Y, Zhao Z, Tang C, et al. Computable early *Caenorhabditis elegans* embryo with a phase field model. *PLoS Comput Biol* 2022;18(1):e1009755.
- [58] Santella A, Catena R, Kovacevic I, Shah P, Yu Z, Marquina-Solis J, et al. WormGUIDES: An interactive single cell developmental atlas and tool for collaborative multidimensional data exploration. *BMC Bioinform* 2015;16:189.
- [59] Aydin Z, Murray JI, Waterston RH, Noble WS. Using machine learning to speed up manual image annotation: Application to a 3D imaging protocol for measuring single cell gene expression in the developing *C. elegans* embryo. *BMC Bioinform* 2010;11:84.
- [60] Santella A, Du Z, Nowotschin S, Hadjantonakis A-K, Bao Z. A hybrid blob-slice model for accurate and efficient detection of fluorescence labeled nuclei in 3D. *BMC Bioinform* 2010;11:580.
- [61] Santella A, Du Z, Bao Z. A semi-local neighborhood-based framework for probabilistic cell lineage tracing. *BMC Bioinform* 2014;15:217.
- [62] Katzman B, Tang D, Santella A, Bao Z. AceTree: A major update and case study in the long term maintenance of open-source scientific software. *BMC Bioinform* 2018;19:121.
- [63] Hunt-Newbury R, Viveiros R, Johnsen R, Mah A, Anastas D, Fang L, et al. High-throughput in vivo analysis of gene expression in *Caenorhabditis elegans*. *PLoS Biol* 2007;5(9):e237.
- [64] Murray JI, Bao Z, Boyle TJ, Boeck ME, Mericle BL, Nicholas TJ, et al. Automated analysis of embryonic gene expression with cellular resolution in *C. elegans*. *Nat Methods* 2008;5(8):703–9.
- [65] Murray JI, Boyle TJ, Preston E, Vafeados D, Mericle B, Weisdepp P, et al. Multidimensional regulation of gene expression in the *C. elegans* embryo. *Genome Res* 2012;22(7):1282–94.
- [66] Murray JI, Bao Z. Automated lineage and expression profiling in live *Caenorhabditis elegans* embryos. *Cold Spring Harb Protoc* 2012:887–99.

- [67] Guan G, Fang M, Wong M-K, Ho VWS, An X, Tang C, et al. Multilevel regulation of muscle-specific transcription factor *h1h-1* during *Caenorhabditis elegans* embryogenesis. *Dev Genes Evol* 2020;230(4):265–78.
- [68] Du Z, Santella A, He F, Tiongson M, Bao Z. De novo inference of systems-level mechanistic models of development from live-imaging-based phenotype analysis. *Cell* 2014;156(1–2):359–72.
- [69] Huang X-T, Zhu Y, Chan LHL, Zhao Z, Yan H. Inference of cellular level signaling networks using single-cell gene expression data in *Caenorhabditis elegans* reveals mechanisms of cell fate specification. *Bioinformatics* 2017;33(10):1528–35.
- [70] Huang X-T, Chan LHL, Zhao Z, Yan H. Gene regulatory effects inference for cell fate determination based on single-cell resolution data. In: 2015 International Conference on Machine Learning and Cybernetics (ICMLC). IEEE; 2015. p. 283–8.
- [71] Zhao Z, Boyle TJ, Bao Z, Murray JI, Mericle B, Waterston RH. Comparative analysis of embryonic cell lineage between *Caenorhabditis briggsae* and *Caenorhabditis elegans*. *Dev Biol* 2008;314(1):93–9.
- [72] Memar N, Schiemann S, Hennig C, Findeis D, Conradt B, Schnabel R. Twenty million years of evolution: The embryogenesis of four *Caenorhabditis* species are indistinguishable despite extensive genome divergence. *Dev Biol* 2019;447(2):182–99.
- [73] Guan G, Wong M-K, Chan L-Y, Ho VWS, An X, Zhao Z, et al. Investigating spatio-temporal cellular interactions in embryonic morphogenesis by 4D nucleus tracking and systematic comparative analysis - Taking nematodes *C. elegans* and *C. briggsae* as examples. In: 2021 IEEE 9th International Conference on Bioinformatics and Computational Biology (ICBCB). IEEE; 2021. p. 6–14.
- [74] Moore JL, Du Z, Bao Z. Systematic quantification of developmental phenotypes at single-cell resolution during embryogenesis. *Development* 2013;140(15):3266–74.
- [75] Guan G, Wong M-K, Ho VWS, An X, Chan L-Y, Tian B, et al. System-level quantification and phenotyping of early embryonic morphogenesis of *Caenorhabditis elegans*. *bioRxiv* 2019. <https://doi.org/10.1101/776062>.
- [76] Cao J, Guan G, Ho VWS, Wong M-K, Chan L-Y, Tang C, et al. Establishment of a morphological atlas of the *Caenorhabditis elegans* embryo using deep-learning-based 4D segmentation. *Nat Commun* 2020;11:6254.
- [77] Guignard L, Fídza U-M, Leggio B, Laussu J, Faure E, Michelin G, et al. Contact area-dependent cell communication and the morphological invariance of ascidian embryogenesis. *Science* 2020;369(6500):eaar5663.
- [78] Fujii Y, Koizumi WC, Imai T, Yokobori M, Matsuo T, Oka K, et al. Spatiotemporal dynamics of single cell stiffness in the early developing ascidian chordate embryo. *Commun Biol* 2021;4:341.
- [79] Zhang S, Teng X, Toyama Y, Saunders TE. Periodic oscillations of Myosin-II mechanically proofread cell-cell connections to ensure robust formation of the cardiac vessel. *Curr Biol* 2020;30(17):3364–77.
- [80] Dye NA, Popović M, Iyer KV, Fuhrmann JF, Piscitello-Gómez R, Eaton S, et al. Self-organized patterning of cell morphology via mechanosensitive feedback. *eLife* 2021;10:e57964.
- [81] Mongera A, Rowghanian P, Gustafson HJ, Shelton E, Kealhofer DA, Carn EK, et al. A fluid-to-solid jamming transition underlies vertebrate body axis elongation. *Nature* 2018;561:401–5.
- [82] Petridou NI, Corominas-Murtra B, Heisenberg C-P, Hannezo E. Rigidity percolation uncovers a structural basis for embryonic tissue phase transitions. *Cell* 2021;184(7):1914–28.
- [83] Klopffer A. On mechanics and morphology. *Nat Phys* 2011;7:672.
- [84] Goodwin K, Nelson CM. Mechanics of development. *Dev Cell* 2021;56(2):240–50.
- [85] Maduro MF. Gut development in *C. elegans*. *Semin Cell Dev Biol* 2017;66:3–11.
- [86] Brandt JN, Voss L, Rambo FM, Nicholson K, Thein JR, Fairchild L, et al. Asymmetric organelle positioning during epithelial polarization of *C. elegans* intestinal cells. *Dev Biol* 2022;481:75–94.
- [87] Pohl C, Bao Z. Chiral forces organize left-right patterning in *C. elegans* by uncoupling midline and anteroposterior axis. *Dev Cell* 2010;19(3):402–12.
- [88] Pohl C. Left-right patterning in the *C. elegans* embryo: Unique mechanisms and common principles. *Commun Integr Biol* 2011;4(1):34–40.
- [89] Arata Y, Takagi H, Sako Y, Sawa H. Power law relationship between cell cycle duration and cell volume in the early embryonic development of *Caenorhabditis elegans*. *Front Physiol* 2015;5:529.
- [90] Fickentscher R, Struntz P, Weiss M. Setting the clock for fail-safe early embryogenesis. *Phys Rev Lett* 2016;117(18):188101.
- [91] Fickentscher R, Krauss SW, Weiss M. Anti-correlation of cell volumes and cell-cycle times during the embryogenesis of a simple model organism. *New J Phys* 2018;20:113001.
- [92] Guan G, Wong M-K, Zhao Z, Tang L-H, Tang C. Volume segregation programming in a nematode's early embryogenesis. *Phys Rev E* 2021;104(5):054409.
- [93] Walston T, Tuskey C, Edgar L, Hawkins N, Ellis G, Bowerman B, et al. Multiple Wnt signaling pathways converge to orient the mitotic spindle in early *C. elegans* embryos. *Dev Cell* 2004;7(6):831–41.
- [94] Goldstein B. Cell contacts orient some cell division axes in the *Caenorhabditis elegans* embryo. *J Cell Biol* 1995;129(4):1071–80.
- [95] Sugioka K, Bowerman B. Combinatorial contact cues specify cell division orientation by directing cortical myosin flows. *Dev Cell* 2018;46(3):257–70.
- [96] Hsu CR, Xiong R, Sugioka K. In vitro reconstitution of spatial cell contact patterns with isolated *Caenorhabditis elegans* embryo blastomeres and adhesive polystyrene beads. *J Vis Exp* 2019;153:e60422.
- [97] Bignone FA. Structural complexity of early embryos: A study on the nematode *Caenorhabditis elegans*. *J Biol Phys* 2001;27(2–3):257–83.
- [98] Voronoi G. Nouvelles applications des paramètres continus à la théorie des formes quadratiques. Premier mémoire. Sur quelques propriétés des formes quadratiques positives parfaites. *Journal für die reine und angewandte Mathematik* 1908;133:97–178.
- [99] Delaunay B. Sur la sphère vide: A la mémoire de Georges Voronoi. *Bulletin de l'Académie des Sciences de l'URSS - Classe des sciences mathématiques et naturelles* 1934;6:793–800.
- [100] Liebling TM, Pournin L. Voronoi diagrams and Delaunay triangulations: Ubiquitous siamese twins. *Documenta Mathematica, ISMP* 2012:419–31.
- [101] Jeon KW. International Review of Cytology: A Survey of Cell Biology (Volume 234). Elsevier Academic Press; 2004.
- [102] Krämer A. Topological coding and visualization grammar of the development of *C. elegans*. In: The 6th World Multi-Conference on Systemics, Cybernetics and Informatics (SCI). International Institute of Informatics and Systemics; 2002.
- [103] Smallwood RH, Holcombe WML, Walker DC. Development and validation of computational models of cellular interaction. *J Mol Histol* 2004;35(7):659–65.
- [104] Hench J, Henriksson J, Lüppert M, Bürglin TR. Spatio-temporal reference model of *Caenorhabditis elegans* embryogenesis with cell contact maps. *Dev Biol* 2009;333(1):1–13.
- [105] Giurumescu CA, Kang S, Planchon TA, Betzig E, Bloomekatz J, Yelon D, et al. Quantitative semi-automated analysis of morphogenesis with single-cell resolution in complex embryos. *Development* 2012;139(22):4271–9.
- [106] Hench J, Henriksson J, Abou-Zied AM, Lüppert M, Dethlefsen J, Mukherjee K. The Homeobox genes of *Caenorhabditis elegans* and insights into their spatio-temporal expression dynamics during embryogenesis. *PLoS ONE* 2015;10(5):e0126947.
- [107] Jelier R, Kruger A, Swoger J, Zimmermann T, Lehner B. Compensatory cell movements confer robustness to mechanical deformation during embryonic development. *Cell Syst* 2016;3(2):160–71.
- [108] Wang Z, Wang D, Li H, Bao Z. Cell neighbor determination in the metazoan embryo system. In: The 8th ACM International Conference on Bioinformatics, Computational Biology, and Health Informatics (ACM-BCB). Association for Computing Machinery; 2017. p. 305–12.
- [109] Chen L, Ho VWS, Wong M-K, Huang X, Chan L-Y, Ng HCK, et al. Establishment of signaling interactions with cellular resolution for every cell cycle of embryogenesis. *Genetics* 2018;209(1):37–49.
- [110] Li X, Zhao Z, Xu W, Fan R, Xiao L, Ma X, et al. Systems properties and spatiotemporal regulation of cell position variability during embryogenesis. *Cell Rep* 2019;26(2):313–21.
- [111] Barnes KM, Fan L, Moyle MW, Brittin CA, Xu Y, Colón-Ramos DA, et al. Cadherin preserves cohesion across involuting tissues during *C. elegans* neurulation. *eLife* 2020;9:e58626.
- [112] Moretti B, Alvarez SNR, Grecco HE. Automatic inference of cell neighborhood in 2D and 3D using nuclear markers. *bioRxiv* 2021. <https://doi.org/10.1101/2021.07.14.452382>.
- [113] Wang Z, Xu Y, Wang D, Yang J, Bao Z. Hierarchical deep reinforcement learning reveals a modular mechanism of cell movement. *Nat Mach Intell* 2022;4:73–83.
- [114] Kaliman S, Jayachandran C, Rehfeldt F, Smith A-S. Limits of applicability of the Voronoi tessellation determined by centers of cell nuclei to epithelium morphology. *Front Physiol* 2016;7:551.
- [115] Pecreaux J, Röper J-C, Kruse K, Jülicher F, Hyman AA, Grill SW, et al. Spindle oscillations during asymmetric cell division require a threshold number of active cortical force generators. *Curr Biol* 2006;16(21):2111–22.
- [116] Cohen-Fix O, Askjaer P. Cell biology of the *Caenorhabditis elegans* nucleus. *Genetics* 2017;205(1):25–59.
- [117] Nance J, Priess JR. Cell polarity and gastrulation in *C. elegans*. *Development* 2002;129(2):387–97.
- [118] Harrell JR, Goldstein B. Internalization of multiple cells during *C. elegans* gastrulation depends on common cytoskeletal mechanisms but different cell polarity and cell fate regulators. *Dev Biol* 2011;350(1):1–12.
- [119] Azuma Y, Onami S. Biologically constrained optimization based cell membrane segmentation in *C. elegans* embryos. *BMC Bioinform* 2017;18:307.
- [120] Cao J, Wong M-K, Zhao Z, Yan H. 3DMMS: Robust 3D membrane morphological segmentation of *C. elegans* embryo. *BMC Bioinform* 2019;20:176.
- [121] Xiong R, Sugioka K. Improved 3D cellular morphometry of *Caenorhabditis elegans* embryos using a refractive index matching medium. *PLoS ONE* 2020;15(9):e0238955.
- [122] Thiels W, Smeets B, Cuvelier M, Caroti F, Jelier R. spherestDT/Mpacts-PiCS: Cell tracking and shape retrieval in membrane-labeled embryos. *Bioinformatics* 2021;37(24):4851–6.
- [123] Odenthal T, Smeets B, Van Liedekerke P, Tijssens E, Van Oosterwyck H, Ramon H. Analysis of initial cell spreading using mechanistic contact formulations for a deformable cell model. *PLoS Comput Biol* 2013;9(10):e100267.
- [124] Smeets B, Cuvelier M, Pešek J, Ramon H. The effect of cortical elasticity and active tension on cell adhesion mechanics. *Biophys J* 2019;116(5):930–7.

- [125] Fujita M, Onami S. Cell-to-cell heterogeneity in cortical tension specifies curvature of contact surfaces in *Caenorhabditis elegans* embryos. *PLoS ONE* 2012;7(1):e30224.
- [126] Xu M, Wu Y, Shroff H, Wu M, Mani M. A scheme for 3-dimensional morphological reconstruction and force inference in the early *C. elegans* embryo. *PLoS ONE* 2018;13(7):e0199151.
- [127] Eschweiler D, Spina TV, Choudhury RC, Meyerowitz E, Cunha A, Stegmaier J. CNN-based preprocessing to optimize watershed-based cell segmentation in 3D confocal microscopy images. In: 2019 IEEE 16th International Symposium on Biomedical Imaging (ISBI). IEEE; 2019. p. 223–7.
- [128] McQuin C, Goodman A, Chernyshev V, Kametsky L, Cimini BA, Karhohs KW, et al. CellProfiler 3.0: Next-generation image processing for biology. *PLoS Biol* 2018;16(7):e2005970.
- [129] Quan TM, Hildebrand DGC, Jeong W-K. FusionNet: A deep fully residual convolutional neural network for image segmentation in connectomics. *Front Comput Sci* 2021;3:613981.
- [130] Stegmaier J, Amat F, Lemon WC, McDole K, Wan Y, Teodoro G, et al. Real-time three-dimensional cell segmentation in large-scale microscopy data of developing embryos. *Dev Cell* 2016;36(2):225–40.
- [131] Wang W, Taft DA, Chen Y-J, Zhang J, Wallace CT, Xu M, et al. Learn to segment single cells with deep distance estimator and deep cell detector. *Comput Biol Med* 2019;108:133–41.
- [132] Chisholm AD, Hardin J. Epidermal morphogenesis. *WormBook* 2005.
- [133] Chen L, Chan LHL, Zhao Z, Yan H. A novel cell nuclei segmentation method for 3D *C. elegans* embryonic time-lapse images. *BMC Bioinform* 2013;14:328.
- [134] Mace DL, Weisdepp P, Gevirtzman L, Boyle T, Waterston RH. A high-fidelity cell lineage tracing method for obtaining systematic spatiotemporal gene expression patterns in *Caenorhabditis elegans*. *G3 Genes/Genomes/Genetics* 2013;3(5):851–63.
- [135] An X, Shao J, Zhang H, Ren X, Ho VWS, Li R, et al. Comparative proteome analysis between *C. briggsae* embryos and larvae reveals a role of chromatin modification proteins in embryonic cell division. *Sci Rep* 2017;7:4296.
- [136] Huisken J, Swoger J, Bene FD, Wittbrodt J, Stelzer EHK. Optical sectioning deep inside live embryos by selective plane illumination microscopy. *Science* 2004;305(5686):1007–9.
- [137] Santi PA. Light sheet fluorescence microscopy: A review. *J Histochem Cytochem* 2011;59(2):129–38.
- [138] Wu Y, Shroff H. Faster, sharper, and deeper: Structured illumination microscopy for biological imaging. *Nat Method* 2018;15:1011–9.
- [139] Ma Y, Wen K, Liu M, Zheng J, Chu K, Smith ZJ, et al. Recent advances in structured illumination microscopy. *J Phys Photonics* 2021;3(2):024009.
- [140] Wu Y, Ghitani A, Christensen R, Santella A, Du Z, Rondeau G, et al. Inverted selective plane illumination microscopy (iSPIM) enables coupled cell identity lineage and neurodevelopmental imaging in *Caenorhabditis elegans*. *Proc Natl Acad Sci U S A* 2011;108(43):17708–13.
- [141] Christensen RP, Bokinsky A, Santella A, Wu Y, Marquina-Solis J, Guo M, et al. Untwisting the *Caenorhabditis elegans* embryo. *eLife* 2015;4:e10070.
- [142] Wu Y, Wawrzusin P, Senseney J, Fischer RS, Christensen R, Santella A, et al. Spatially isotropic four-dimensional imaging with dual-view plane illumination microscopy. *Nat Biotechnol* 2013;31(11):1032–8.
- [143] Kumar A, Wu Y, Christensen R, Chandris P, Gandler W, McCreedy E, et al. Dual-view plane illumination microscopy for rapid and spatially isotropic imaging. *Nat Protoc* 2014;9(11):2555–73.
- [144] Kumar A, Christensen R, Guo M, Chandris P, Duncan W, Wu Y, et al. Using stage- and slit-scanning to improve contrast and optical sectioning in dual-view inverted light sheet microscopy (diSPIM). *Biol Bull* 2016;231(1):26–39.
- [145] Duncan LH, Moyle MW, Shao L, Sengupta T, Ikegami R, Kumar A, et al. Isotropic light-sheet microscopy and automated cell lineage analyses to catalogue *Caenorhabditis elegans* embryogenesis with subcellular resolution. *J Vis Exp* 2019;148:e59533.
- [146] Shah PK, Santella A, Jacobo A, Siletti K, Hudspeth AJ, Bao Z. An *in toto* approach to dissecting cellular interactions in complex tissues. *Dev Cell* 2017;43(4):530–40.
- [147] Ohno H, Bao Z. Small RNAs couple embryonic developmental programs to gut microbes. *Sci Adv* 2022;8(12):eab17663.
- [148] Meinertzhagen IA. Eutely, cell lineage, and fate within the ascidian larval nervous system: determinacy or to be determined? *Can J Zool* 2005;83(1):184–95.
- [149] Dumollard R, Minc N, Salez G, Aicha SB, Bekkouche F, Hebras C, et al. The invariant cleavage pattern displayed by ascidian embryos depends on spindle positioning along the cell's longest axis in the apical plane and relies on asynchronous cell divisions. *eLife* 2017;6:e19290.
- [150] Faure E, Savy T, Rizzi B, Melani C, Stašová O, Fabrèges D, et al. A workflow to process 3D+time microscopy images of developing organisms and reconstruct their cell lineage. *Nat Commun* 2016;7:8674.
- [151] Hartenstein V. Atlas of *Drosophila* Development. Cold Spring Harbor Laboratory Press; 1993.
- [152] Gilbert SF. Developmental Biology. 6th edition. Sinauer Associates; 2000.
- [153] Amat F, Lemon W, Mossing DP, McDole K, Wan Y, Branson K, et al. Fast, accurate reconstruction of cell lineages from large-scale fluorescence microscopy data. *Nat Methods* 2014;11(9):951–8.
- [154] Khan Z, Wang Y-C, Wieschaus EF, Kaschube M. Quantitative 4D analyses of epithelial folding during *Drosophila* gastrulation. *Development* 2014;141(14):2895–900.
- [155] Kimmel CB, Ballard WW, Kimmel SR, Ullmann B, Schilling TF. Stages of embryonic development of the zebrafish. *Dev Dyn* 1995;203(3):253–310.
- [156] McDougall A, Chenevert J, Dumollard R. Cell-cycle control in oocytes and during early embryonic cleavage cycles in ascidians. *Int Rev Cell Mol Biol* 2012;297:235–64.
- [157] Tadros W, Lipshitz HD. The maternal-to-zygotic transition: A play in two acts. *Development* 2009;136(18):3033–42.
- [158] Vastenhouw NL, Cao WX, Lipshitz HD. The maternal-to-zygotic transition revisited. *Development* 2019;146(11):dev161471.
- [159] Rose L, Gönczy P. Polarity establishment, asymmetric division and segregation of fate determinants in early *C. elegans* embryos. *WormBook* 2014.
- [160] Jankele R, Jelier R, Gönczy P. Physically asymmetric division of the *C. elegans* zygote ensures invariably successful embryogenesis. *eLife* 2021;10:e61714.
- [161] Goldstein B, Macara IG. The PAR proteins: Fundamental players in animal cell polarization. *Dev Cell* 2007;13(5):609–22.
- [162] Griffin EE. Cytoplasmic localization and asymmetric division in the early embryo of *Caenorhabditis elegans*. *WIREs Dev Biol* 2015;4(3):267–82.
- [163] Hubatsch L, Peglion F, Reich JD, Rodrigues NT, Hirani N, Illukkumbura R, et al. A cell-size threshold limits cell polarity and asymmetric division potential. *Nat Phys* 2019;15:1075–85.
- [164] Goldstein B, Hird SN. Specification of the anteroposterior axis in *Caenorhabditis elegans*. *Development* 1996;122(5):1467–74.
- [165] Boxem M, van de Heuvel S. Cell polarity: Getting the PARty started. *Curr Biol* 2019;29(13):R637–9.
- [166] Gubieda AG, Packer JR, Squires I, Martin J, Rodriguez J. Going with the flow: Insights from *Caenorhabditis elegans* zygote polarization. *Philos Trans R Soc Lond B Biol Sci* 2020;375(1809):20190555.
- [167] Cuenca AA, Schetter A, Aceto D, Kempthues K, Seydoux G. Polarization of the *C. elegans* zygote proceeds via distinct establishment and maintenance phases. *Development* 2003;130(7):1255–65.
- [168] Gardner TS, Cantor CR, Collins JJ. Construction of a genetic toggle switch in *Escherichia coli*. *Nature* 2000;403:339–42.
- [169] Elowitz MB, Leibler S. A synthetic oscillatory network of transcriptional regulators. *Nature* 2000;403:335–8.
- [170] Alon U. An introduction to systems biology: Design principles of biological circuits. Chapman and Hall/CRC; 2006.
- [171] Ma W, Trusina A, El-Samad H, Lim WA, Tang C. Defining network topologies that can achieve biochemical adaptation. *Cell* 2009;138(4):760–73.
- [172] Chau AH, Walter JM, Gerardin J, Tang C, Lim WA. Designing synthetic regulatory networks capable of self-organizing cell polarization. *Cell* 2012;151(2):320–32.
- [173] Goehring NW, Hoegge C, Grill SW, Hyman AA. PAR proteins diffuse freely across the anterior-posterior boundary in polarized *C. elegans* embryos. *J Cell Biol* 2011;193(3):583–94.
- [174] Seirin-Lee S. Asymmetric cell division from a cell to cells: Shape, length, and location of polarity domain. *Dev Growth Differ* 2020;62(3):188–95.
- [175] Tostevin F, Howard M. Modeling the establishment of PAR protein polarity in the one-cell *C. elegans* embryo. *Biophys J* 2008;95(10):4512–22.
- [176] Goehring NW, Trong PK, Bois JS, Chowdhury D, Nicola EM, Hyman AA, et al. Polarization of PAR proteins by advective triggering of a pattern-forming system. *Science* 2011;334(6059):1137–41.
- [177] Bois JS, Grill SW. Mechanochemical pattern formation in the polarization of the one-cell *C. elegans* embryo. *World Scientific Lecture Notes in Complex System - Engineering of Chemical Complexity* 2013:201–12.
- [178] Kravtsova N, Dawes AT. Actomyosin regulation and symmetry breaking in a model of polarization in the early *Caenorhabditis elegans* embryo: Symmetry breaking in cell polarization. *Bull Math Biol* 2014;76(10):2426–48.
- [179] Seirin-Lee S, Shibata T. Self-organization and advective transport in the cell polarity formation for asymmetric cell division. *J Theor Biol* 2015;382:1–14.
- [180] Seirin-Lee S, Sukekawa T, Nakahara T, Ishii H, Ei S-I. Transitions to slow or fast diffusions provide a general property for in-phase or anti-phase polarity in a cell. *J Math Biol* 2020;80(6):1885–917.
- [181] Gross P, Kumar KV, Goehring NW, Bois JS, Hoegge C, Jülicher F, et al. Guiding self-organized pattern formation in cell polarity establishment. *Nat Phys* 2019;15:293–300.
- [182] Lim YW, Wen F-L, Shankar P, Shibata T, Motegi F. A balance between antagonizing PAR proteins specifies the pattern of asymmetric and symmetric divisions in *C. elegans* embryogenesis. *Cell Rep* 2021;36(1):109326.
- [183] Dawes AT, Iron D. Cortical geometry may influence placement of interface between Par protein domains in early *Caenorhabditis elegans* embryos. *J Theor Biol* 2013;333:27–37.
- [184] Aras BS, Zhou YC, Dawes A, Chou C-S. The importance of mechanical constraints for proper polarization and pseudo-cleavage furrow generation in the early *Caenorhabditis elegans* embryo. *PLoS Comput Biol* 2018;14(7):e1006294.
- [185] Geßle R, Halatek J, Würthner L, Frey E. Geometric cues stabilise long-axis polarisation of PAR protein patterns in *C. elegans*. *Nat Commun* 2020;11:539.
- [186] Morita Y, Seirin-Lee S. Long time behavior and stable patterns in high-dimensional polarity models of asymmetric cell division. *J Math Biol* 2021;82(7):66.
- [187] Dawes AT, Munro EM. PAR-3 oligomerization may provide an actin-independent mechanism to maintain distinct par protein domains in the early *Caenorhabditis elegans* embryo. *Biophys J* 2011;101(6):1412–22.
- [188] Seirin-Lee S, Gaffney EA, Dawes AT. CDC-42 interactions with Par proteins are critical for proper patterning in polarization. *Cells* 2020;9(9):2036.

- [189] Seirin-Lee S. The role of cytoplasmic MEX-5/6 polarity in asymmetric cell division. *Bull Math Biol* 2021;83(4):29.
- [190] Seirin-Lee S. Positioning of polarity formation by extracellular signaling during asymmetric cell division. *J Theor Biol* 2016;400:52–64.
- [191] Hoeghe C, Hyman AA. Principles of PAR polarity in *Caenorhabditis elegans* embryos. *Nat Rev Mol Cell Biol* 2013;14:315–22.
- [192] Kajita A, Yamamura M, Kohara Y. Computer simulation of the cellular arrangement using physical model in early cleavage of the nematode *Caenorhabditis elegans*. *Bioinformatics* 2003;19(6):704–16.
- [193] Kajita A, Yamamura M, Kohara Y. Physical modeling of the cellular arrangement in *C. elegans* early embryo: Effect of rounding and stiffening of the cells. *Genome Inform* 2002;13:224–32.
- [194] Fickentscher R, Struntz P, Weiss M. Mechanical cues in the early embryogenesis of *Caenorhabditis elegans*. *Biophys J* 2013;105(8):1805–11.
- [195] Tian B, Guan G, Tang L-H, Tang C. Why and how the nematode's early embryogenesis can be precise and robust: A mechanical perspective. *Phys Biol* 2020;17(2):026001.
- [196] Yamamoto K, Kimura A. An asymmetric attraction model for the diversity and robustness of cell arrangement in nematodes. *Development* 2017;144(23):4437–49.
- [197] Kikuchi Y, Kimura A. Microinjection into the *Caenorhabditis elegans* embryo using an uncoated glass needle enables cell lineage visualization and reveals cell-non-autonomous adhesion control. *bioRxiv* 2018. <https://doi.org/10.1101/406991>.
- [198] Giammona J, Campàs O. Physical constraints on early blastomere packings. *PLoS Comput Biol* 2021;17(1):e1007994.
- [199] Kimura A. *Quantitative Biology - A Practical Introduction*. Springer; 2022.
- [200] Miao J, Guan G, Tang C. Spontaneous mechanical and energetic state transitions during *Caenorhabditis elegans* gastrulation. *arXiv* 2022. <https://arxiv.org/abs/2105.05795>.
- [201] Guan G, Tang L-H, Tang C. Reconstructing the multicellular structure of a developing metazoan embryo with repulsion-attraction model and cell-cell connection atlas *in vivo*. *J Phys: Conf Ser* 2020;1592:012020.
- [202] van der Waals JD. Thermodynamische theorie der kapillarität unter voraussetzung stetiger dichteänderung. *Z Phys Chem* 1894;13:657–725.
- [203] Cahn JW, Hilliard JE. Free energy of a nonuniform system. I. Interfacial free energy. *J Chem Phys* 1958;28(2):258–67.
- [204] Chen L-Q. Phase-field models for microstructure evolution. *Annu Rev Mater Res* 2002;32:113–40.
- [205] Boettinger WJ, Warren JA, Beckermann C, Karma A. Phase-field simulation of solidification. *Annu Rev Mater Res* 2002;32:163–94.
- [206] Moure A, Gomez H. Phase-field model of cellular migration: Three-dimensional simulations in fibrous networks. *Comput Method Appl M* 2017;320:162–97.
- [207] Cao Y, Ghabache E, Rappel W-J. Plasticity of cell migration resulting from mechanochemical coupling. *eLife* 2019;8:e48478.
- [208] Jiang J, Garikipati K, Rudraraju S. A diffuse interface framework for modeling the evolution of multi-cell aggregates as a soft packing problem driven by the growth and division of cells. *Bull Math Biol* 2019;81(8):3282–300.
- [209] Dutta P, Oedra D, Pohl C. Planar asymmetries in the *C. elegans* embryo emerge by differential retention of aPARs at cell-cell contacts. *Front Cell Dev Biol* 2019;7:209.
- [210] Kuang X, Guan G, Tang C, Zhang L. *MorphoSim*: An efficient and scalable phase-field framework for accurately simulating multicellular morphologies. *arXiv* 2022. <https://arxiv.org/abs/2206.04903>.
- [211] Seirin-Lee S, Yamamoto K, Kimura A. The extra-embryonic space and the local contour are crucial geometric constraints regulating cell arrangement. *Development* 2022;149(9):dev200401.
- [212] Brauchle M, Baumer K, Gönczy P. Differential activation of the DNA replication checkpoint contributes to asynchrony of cell division in *C. elegans* embryos. *Curr Biol* 2003;13(10):819–27.
- [213] Way M. "What I cannot create, I do not understand". *J Cell Sci* 2017;130(18):2941–2.
- [214] Wolpert L. Do we understand development?. *Science* 1994;266(5185):571–2.
- [215] Biasuz K, Leggio B, Faure E, Lemaire P. The "computable egg": Myth or useful concept?. *Curr Opin Syst Biol* 2018;11:91–7.